

## High-volume recycled glass cementitious and geopolymer composites incorporating graphene oxide

Nghia P. Tran<sup>1</sup>, Tianchun Wang<sup>\*,1</sup>, Tuan N. Nguyen<sup>\*,1</sup>, Hesong Jin, Tuan D. Ngo

*Department of Infrastructure Engineering, The University of Melbourne, VIC 3010, Australia*

### ARTICLE INFO

**Keywords:**

High-volume waste glass  
Graphene oxide (GO)  
Alkali-activated materials  
Cement-based materials  
Alkali-silica reaction (ASR)  
Sustainability

### ABSTRACT

This study presents the development of high-volume recycled glass construction materials using recycled glass aggregate (RGA) as a 100 % sand replacement, recycled glass powder (RGP) as 40 wt% of the binder, and 0.1 wt % graphene oxide (GO) as nano-reinforcement. The research investigates the individual and their combined effects on the engineering performance, reaction kinetics (using calorimetry, X-ray diffraction-XRD, Fourier Transform Infrared-FTIR and Thermogravimetric analysis-TGA), and microstructure (Scanning Electron Microscopy/ Energy Dispersive X-ray Spectroscopy-SEM/EDS) for both cementitious and geopolymer systems. The results indicate that while RGA reduces strength and exacerbates alkali-silica reaction (ASR), the presence of 40 wt% RGP significantly mitigates ASR despite a lower strength gain in both systems. Geopolymers exhibit significantly lower ASR expansion compared to cementitious matrices owing to their superior alkali-binding capacity and denser microstructure, which restricts water and alkali ion mobility. 0.1 wt% GO was found to accelerate geopolymerisation, enhancing the strength of geopolymer mixes, but it decreased compressive strength in cement-based mixes due to self-desiccation-induced micro-cracking under ambient curing condition. The study also highlights that cement and metasilicate, as well as slag, are the main contributors to cost and CO<sub>2</sub> emissions in cementitious and geopolymer systems, respectively. Overall, geopolymers exhibit a significantly lower global warming potential (< 180 kg CO<sub>2</sub>-eq/m<sup>3</sup>) compared to cement-based mixes (> 365 kg CO<sub>2</sub>-eq/m<sup>3</sup>) with a comparable cost (190–230 AUD/m<sup>3</sup>). The results indicate the potential for sustainable construction applications using high volumes of recycled glass, incorporating over 70 % of the mixture by weight.

### 1. Introduction

Waste glass has become a substantial proportion of solid waste stream, and its disposal is recognised as a global issue [1]. Due to its inert characteristic, glass can technically be recycled infinitely and remelted to manufacture new glass products after its service life. Nonetheless, this ideal situation rarely achieved due to contamination and the mixing of different glass colours and types in the waste stream [2]. The recycling rate for waste glass varies significantly among different countries and regions, reaching 67 % in Turkey [3] and 57 % in Australia [4], but only 24 % in US [5] and 8 % in Hong Kong [6]. It is estimated that around 200 million tonnes of waste glass end up in landfills globally each year [7]. Since waste glass is non-biodegradable it accumulates in landfills over the long term, posing substantial environmental hazards and contributing to the growing waste management crisis [2,8]. On the other hand, cement and concrete industry faces

significant challenges due to the immense demand of concrete, the most widely used man-made material worldwide [9]. Cement manufacturing is responsible for 8–9 % of the global anthropogenic CO<sub>2</sub> emission [10], highlighting the urgent need for decarbonisation to achieve net zero emissions by 2050.

To address the concurrent issues in waste glass management and the concrete industry, extensive research has been conducted to incorporate recycled glass aggregate (RGA) as sand replacement [11,12] or recycled glass powders (RGP) as additives [13] in Ordinary Portland cement (OPC) and geopolymer mortar/concrete. Previous studies have shown that using RGA or RGP can have either beneficial or detrimental effects on mortar/concrete performance, depending on its fineness, shape, texture, and type, among which the fineness has been identified as the principal factor [1,14,15]. Generally, higher fineness increases the pozzolanic reactivity of this material, leading to improved mortar/concrete performance, especially when used as supplementary cementitious materials (SCM) [16–18]. Compared to OPC mortar/concrete,

\* Corresponding authors.

E-mail addresses: [echo.wang@unimelb.edu.au](mailto:echo.wang@unimelb.edu.au) (T. Wang), [tuan.nguyen@unimelb.edu.au](mailto:tuan.nguyen@unimelb.edu.au) (T.N. Nguyen).

<sup>1</sup> Co-author with equal contribution

Nomenclature	
RGA	Recycled glass aggregate.
RGP	Recycled glass powder.
OPC	Ordinary Portland cement.
SCM	Supplementary cementitious materials.
GO	Graphene oxide.
ITZ	Interfacial transition zone.
GGBS	Ground Granulated Blast-Furnace Slag.
FA	Fly ash.
ASR	Alkali-Silica Reaction.
NS	Natural sand.
XRD	X-ray diffraction.
XRF	X-ray fluorescence.
SEM/EDS	Scanning Electron Microscopy/ Energy Dispersive X-ray
SP	Spectroscopy.
W/B	Superplasticier.
A/B	water-to-binder ratio.
TG/DTG	aggregate-to-binder ratio.
FTIR	Thermogravimetric/derivative thermogravimetric.
C-S-H	Fourier Transform Infrared.
C-(A)-S-H	Calcium silicate hydrate.
N-A-S-H	Calcium (alumino)silicate hydrate.
C <sub>3</sub> S	Sodium aluminosilicate hydrate.
C <sub>2</sub> S	Tricalcium silicate (Alite).
AFm	Dicalcium silicate (Belite).
GWP	Hydrated calcium aluminate.
IPCC	Global Warming Potential.
AusLCI	Intergovernmental Panel on Climate Change.
	Australian National Life Cycle Inventory.

the use of recycled glass in geopolymer mortar/concrete is relatively limited. When RGP is used as precursor, the performance of geopolymer mortar/concrete are affected by various factors, including the fineness of the glass, curing time, curing temperature, the concentration of the alkaline solution, and the properties of other precursors blended with RGP [19]. Researchers have also investigated the feasibility of using RGP as the activator for more sustainable geopolymer concrete [20,21]. The primary concern of incorporating waste glass in OPC and geopolymer mortar/concrete is Alkali-Silica Reaction (ASR) due to high amount of amorphous silica in glass (nearly 70%). In OPC mortar/concrete, a “threshold size” was reported for waste glass in a range from 0.3 mm to 1 mm, under which ASR is effectively suppressed due to the beneficial pozzolanic reaction [22–26]. ASR in geopolymer mortar/concrete is more complicated and therefore less extensively studied by the scientific community [19,27,28]. Despite its high alkaline environment, less severe ASR expansion was reported in geopolymer mortar/concrete than OPC mortar/concrete [29]. However, there is a point to take care when highly reactive aggregate used, the amorphous silica in highly reactive aggregate would react with high alkaline activator. Thereby, the ASR would have started during the alkaline activation which would increase the complexity of analysing the ASR behaviour in geopolymer system [28]. It is widely acknowledged that RGP less than 75 microns has been recognised as an ASR inhibitor, which facilitates the co-utilisation of RGF and RGP [18,30–33].

By co-utilisation of RGF and RGP in high volume, the usage of waste glass can be maximised, and the alleviation of waste glass stockpiling and decarbonisation of concrete industry can be further accelerated. However, only a few studies have assessed the behaviour of cementitious mortar/concrete with a combined use of waste glass as fine aggregate and SCM [18,30–33], which requires more research in this area for a more sustainable cement-based construction. Meanwhile, the evaluation its high-volume utilisation in geopolymer mortar/concrete remains even more largely unexplored [19,29]. Furthermore, no research has been conducted to comprehensively compare the performance of cementitious and geopolymer mortar/concrete while incorporating high-volume waste glass as both sand replacement and OPC/precursor replacement. In recent, graphene-based nanosheets have been widely used in concrete for different applications due to its excellent characteristics and functional groups [34]. As a derivative of graphene, graphene oxide (GO) has emerged as a promising nano-additive to improve the performance of OPC composites, thereby promoting cement hydration, refining pore structure, compacting microstructure and improving interfacial bonding with the matrix [35]. Additionally, GO has been proven to be effective in suppressing ASR by reshaping and refining Calcium silicate hydrate (C-S-H) gels around interfacial transition zone (ITZ) through its superior nano-nucleation and interlocking effect [36]. Despite reported positive results, limited

studies have been conducted on GO-modified geopolymer composites [37], especially on the Ground Granulated Blast-Furnace Slag (GGBS) and Fly Ash (FA)-based geopolymer composites. Given the promising effects of GO in enhancing mechanical performance and controlling ASR in both OPC and geopolymer composites, it holds significant potential for use with waste glass in these systems. Some work has been done using GO with waste cathode-ray tube glass but focusing on inhibiting the lead leaching [38,39]. However, to the authors' knowledge, its effects in systems co-utilising RGA and RGP have not been thoroughly investigated.

This study addresses these gaps by, for the first time, developing high-volume recycled glass mortars by including RGA as a 100 wt% sand replacement, RGP as 40 wt% of the binder, and 0.1 wt% GO as nano-scaled reinforcement. This study demonstrated the effects of co-utilising RGA and RGP in high-volume and GO on the engineering properties and sustainability of both cementitious and geopolymer mortars. Their individual and combined effects were assessed on the engineering performance (flowability, compressive strength and ASR expansion), reaction kinetics and microstructure for both cementitious and geopolymer systems. In addition, a comparative environmental and cost analysis were performed on the investigated cementitious and geopolymer mortars, providing insights into the sustainability and feasibility of these innovative materials in construction.

## 2. Significance of research

The most widely-used SCM in cementitious composite or precursor in geopolymer composite are FA [40–42] and GGBS [40–44]. Despite their successful implementation worldwide, there is a growing imbalance between their supply and demand due to reduced steel production and a shift towards cleaner energy sources [45–49]. Additionally, there is an increasing shortage of natural aggregates for concrete production, particularly natural sand (NS) [9]. The environmental impact of excavating NS, including deforestation, ecosystem destruction, and water pollution, is significant [50,51]. Hence, utilising high-volume recycled glass as additive to partially replace cement or geopolymer precursor, and alternative aggregate to substitute NS can be one of the most effective decarbonisation pathways in the future [52,53]. By exploring this dual application, the study not only addresses the critical material shortages but also provides a novel pathway for significant decarbonisation in the concrete industry. The findings offer fresh insights into the engineering performance, cost-effectiveness, and environmental benefits of the developed innovative construction materials, advancing eco-friendly construction practices in line with global sustainability goals.

### 3. Materials, mixing and testing

#### 3.1. Materials

The OPC purchased from Cement Australia was used in the study. The cement particles have an average size D-50 of 17.2  $\mu\text{m}$  and a specific gravity of 3.15. Class F FA from Cement Australia and GGBS from Australian Builders were used in this study. The average size D-50 is 21.2  $\mu\text{m}$  and 12.7  $\mu\text{m}$ , and the specific gravity is 2.45 and 2.80 for FA and GGBS respectively. Before use, all the powdered materials were sieved passing through 850  $\mu\text{m}$  to remove any lumps. NS was purchased from Ararat Building Supplies, Australia, which is classified as unreactive. The specific gravity and water absorption of NS are 2.91 and 0.3 % respectively. RGA was collected from Schneppa Glass, with the specific gravity and water absorption of 2.53 and 0.22 %. Four size fractions of NS and RGA were used in this study which are 150–300  $\mu\text{m}$ , 300–600  $\mu\text{m}$ , 0.6–1.18 mm and 1.18 – 2.36 mm. RGP was achieved by grinding 0.15–0.3 mm glass fines for 2 min by using a ring mill, which has an average size of 11.3  $\mu\text{m}$  and a specific gravity of 2.57. The particle size distribution of OPC, RGP, FA and GGBS were determined through Malvern Mastersizer 3000, as shown in Fig. 1. Their chemical composition was obtained by X-ray fluorescence (XRF) as shown in Table 1. Their X-ray diffraction (XRD) patterns and Scanning Electron Microscopy (SEM) images are also displayed in Fig. 2. Solid metasilicate (modulus ratio of 0.92 and specific gravity of 1.2) was obtained from Redox company. A superplasticizer (SP) made of polycarboxylic ether – namely MasterGlenium SKY 8379 from Master Builder Solutions was used in this study, with a specific gravity of 1.09 [54]. GO in suspension form was purchased from Graphenea with a concentration of 2.5 wt%.

#### 3.2. Mixing procedures

The mixing proportions for cementitious and geopolymer mortar used in this study are summarised in Table 2 and Table 3. A water-to-binder (W/B) ratio 0.4 and aggregate-to-binder ratio (A/B) 2.25 was used in all mortar mixes based on ASTM C 1260 [55] – the standard method for accelerated ASR test. Both NS and RGA consists of four size fractions (150–300  $\mu\text{m}$ , 300–600  $\mu\text{m}$ , 0.6–1.18 mm and 1.18 – 2.36 mm) with the proportion of 15 %, 25 %, 25 %, and 35 %. RGA was used to fully replace NS in both systems. 40 wt% substitution of RGP was investigated by replacing OPC in cementitious system and replacing both FA and GGBS (1:1) in geopolymer system. The dosage of superplasticizer was 1.0 wt% in geopolymer mortar and 0.25 wt% in cementitious mortar. GO of 0.1 wt% was added in both systems to investigate their effects on materials' performance, reaction kinetics and microstructure. It should be noticed that the total water content of the mixture with GO was inclusive of the water present in the GO suspension

to maintain the fixed W/B ratio. In order to obtain well-dispersed aqueous GO solution, GO suspension was first mixed thoroughly with water and SP, which was then sonicated using an ultrasonicator at a power of 300 W for 40 min. The ultrasonicator was operated for 1 s with 1 s intervals between sonication cycles to avert over-heating effects. In this study, several tests were conducted for paste samples (see Section 3.3). Mixing proportions for paste samples follow Table 2 and Table 3 by removing fine aggregate and their denotation starts with OPC-xxx for cement system and GEO-xxx for geopolymer system.

The mixing procedure was similar for either paste or mortar mixtures in both cementitious and geopolymer systems. Firstly, the dry ingredients were initially blended at a slow speed for 2 mins. Following this, a well-dispersed GO solution was gradually incorporated into the dry mixture. The blending process was then extended for an additional 10 mins, with a high-speed mixing interval of 1 min at every 5 mins. The homogeneous mixture was transferred into moulds and compacted using a vibrating table to eliminate entrapped air bubbles. To prevent moisture loss and shrinkage-induced cracking, the surface was covered with cling wrap [56]. After one day of storage in the laboratory, all samples were demolded and stored in sealed plastic bags under ambient conditions until the testing date.

#### 3.3. Testing methodology

The determination of workability of fresh mortar mixture followed ASTM C1437 [57] by measuring the diameter change after the flow table was dropped for 25 times in 15 seconds. The compressive strength was tested on 50 × 50 × 50 mm mortar cubes at the curing age of 28 days according to ASTM C 109 [58]. The accelerated ASR mortar bar test was conducted following ASTM C 1260 [55] and ASTM C 1567 [59] by measuring the expansion of 25 × 25 × 285 mm mortar bars up to 14 days while immersed in 1 N NaOH bath at a temperature of 80 ± 2 °C, as illustrated in Fig. 3. The reference length for the deduction was the length of the mortar bar after being immersed in an 80°C water bath for 24 hours. For each mixture, the thermal expansion of three mortar bars was checked to ensure acceptable variation, making the deductions valid and meaningful before transferring the samples to 80°C 1 N NaOH bath.

Hydration kinetic of the paste was investigated using the TAM Air isothermal calorimeter, at a base temperature of 25 ± 0.02 °C, by recording the heat flow of the first 48 h of the reaction. All values for heat flow were normalised by the weight of material content. Thermogravimetric and derivative thermogravimetric analysis (TG/DTG) was conducted using a PerkinElmer TGA 8000 with a temperature range within 35 – 800 °C, a heating rate of 10 °C/min and a purge rate of 20 mL/min in nitrogen atmosphere. Fourier Transform Infrared (FTIR) spectroscopic analysis was conducted using a ThermoFisher Scientific spectrometer, operating over the spectral range of 400–4000  $\text{cm}^{-1}$ , with potassium bromide used as the reference material. For XRF characterisation, the raw materials in powder form were pressed into pellets before being characterised by Bruker S2 Puma X-ray Fluorescence (XRF) Spectrometer. XRD was performed on the hardened paste at 28 days by using a Bruker D8 Advance Powder Diffractometer using Cu K $\alpha$  radiation between 5° and 60° at 20. The voltage and current were set at 40 kV and 40 mA respectively, with a wavelength of 1.5418 Å. The phases in the XRD patterns were identified using the "ICDD PDF-4+ Scholar 2021" database. The hydrated paste sample was first crushed into small piece after which immersed in iso-propanol solution for 2 days to stop the reaction. After draining the iso-propanol, the paste pieces were dried and grinded into powder passing through 45 microns until being tested. A detail of SEM sample preparation procedure with grinding and polishing process was followed the previous research [60]. SEM coupling Energy Dispersive X-ray Spectroscopy (EDS) was conducted by an FEI Teneo VolumeScope. To achieve high-quality imaging, the experimental setup was configured with a working distance of 10 mm and an accelerating voltage of 30 kV as used in other studies [61,62].

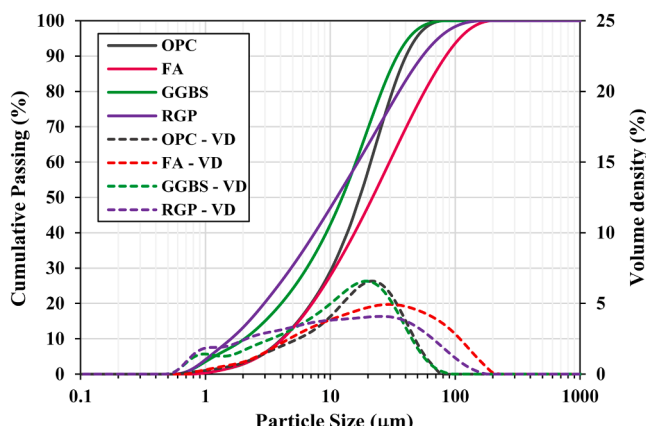


Fig. 1. Particle size distribution of OPC, FA, GGBS and RGP (Solid lines represent cumulative passing %, dashed lines represent volume density (VD)).

**Table 1**

Oxide composition of raw materials determined by XRF.

Materials	SiO <sub>2</sub>	CaO	Na <sub>2</sub> O	Al <sub>2</sub> O <sub>3</sub>	Fe <sub>2</sub> O <sub>3</sub>	SO <sub>3</sub>	K <sub>2</sub> O	TiO <sub>2</sub>	MnO	MgO	P <sub>2</sub> O <sub>5</sub>	LOI
OPC	17.61	68.72	-	3.95	3.34	3.54	0.64	0.20	0.05	1.13	-	0.60
RGP	71.38	9.53	12.94	1.67	0.13	0.17	0.32	0.02	-	3.70	-	0.14
FA	52.75	6.66	-	27.66	8.12	0.52	0.85	1.51	0.11	1.23	0.41	0.18
GGBS	31.17	44.34	-	11.86	0.30	5.13	0.41	0.62	0.28	5.57	-	0.32

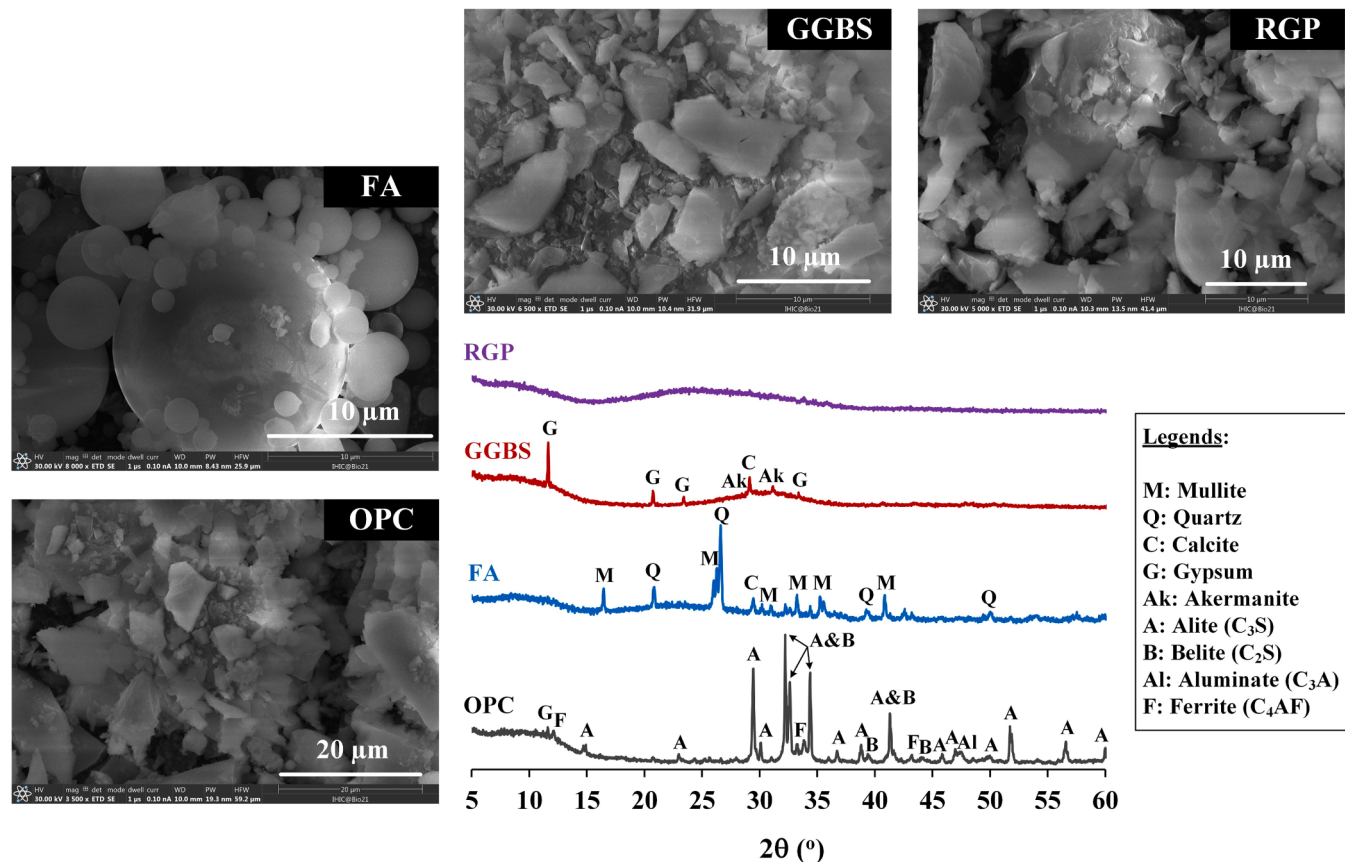


Fig. 2. XRD patterns and SEM images of OPC, FA, GGBS and RGP.

**Table 2**Mixing proportions for cementitious mortar (kg/m<sup>3</sup>).

Mixes	OPC	RGP	GO	RGA	NS	Water	SP	Unit weight
C-S	615.4	-	-	-	1384.7	246.2	1.5	2249.5
C-G	608.5	-	-	1369.2	-	243.4	1.5	2224.3
C-GGP	357.7	238.4	-	1341.3	-	238.4	1.5	2178.9
C-GGPGO	357.6	238.4	0.6	1343.4	-	238.8	1.5	2175.8

Note: C-S: Cement system with sand as fine aggregate; C-G: Cement system with glass as fine aggregate; C-GGP: Cement system with glass as fine aggregate, glass powder as partial cement replacement; C-GGPGO: Cement system with glass as fine aggregate, glass powder as partial cement replacement, reinforced by graphene oxide.

**Table 3**Mixing proportions for geopolymer mortar (kg/m<sup>3</sup>).

Mixes	FA	GGBS	RGP	GO	Meta-silicate	RGA	NS	Water	SP	Unit weight
G-S	281.0	281.0	-	-	56.2	-	1264.3	224.8	5.6	2107.2
G-G	278.1	278.1	-	-	55.6	1251.	-	222.5	5.6	2085.7
G-GGP	166.1	166.1	221.4	-	55.4	1245.5	-	221.4	5.5	2075.9
G-GGPGO	166.0	166.0	221.4	0.6	55.3	1245.2	-	221.4	5.5	2075.9

Note: G-S: Geopolymer system with sand as fine aggregate; G-G: Geopolymer system with glass as fine aggregate; G-GGP: Geopolymer system with glass as fine aggregate, glass powder as partial cement replacement; G-GGPGO: Geopolymer system with glass as fine aggregate, glass powder as partial cement replacement, reinforced by graphene oxide. Paste sample is with GEO-xxx.

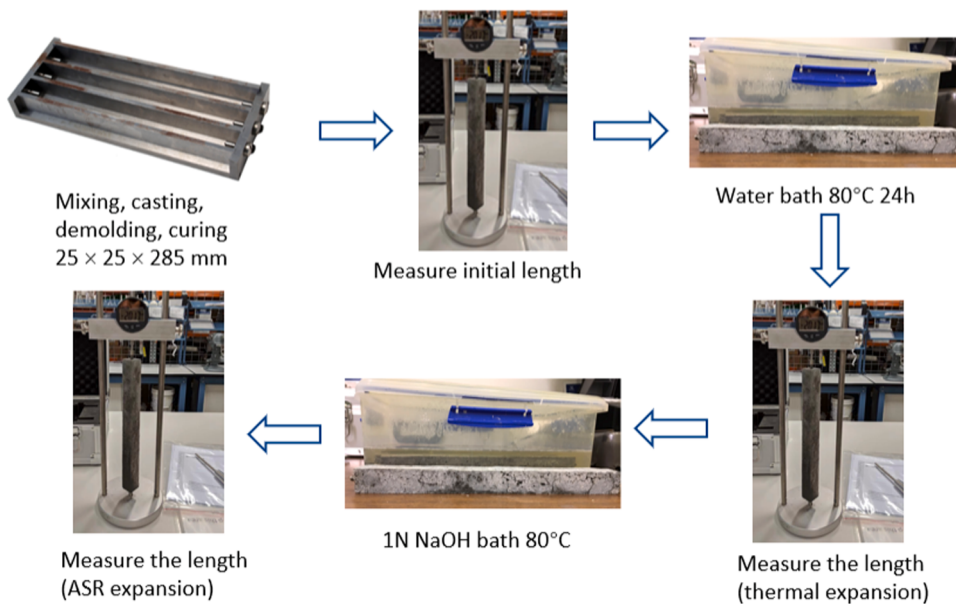


Fig. 3. Accelerated mortar bar test.

### 3.4. Embodied carbon and cost analysis

A comparative environmental and cost analysis were performed on the investigated cementitious and geopolymer mortars. The environmental analysis only focused on carbon footprint from cradle to gate (A1-A3). It is also known as Global Warming Potential (GWP), which is measured in kg CO<sub>2</sub> equivalent as per Intergovernmental Panel on Climate Change (IPCC) Forth Assessment Report with a 100-year time horizon [63]. The GWP and unit cost inventory of all materials are presented in Table 4. The GWP inventory data was predominantly sourced from the latest version of Australian National Life Cycle Inventory (AusLCI) [64]. The unit cost inventory data was collected from various sources including the up-to-date Australian market price and most recent report/publication conducted within Australian context. Therefore, it should be noted that environmental and cost analysis conducted in the present study is limited to current Australian context. For each mix, the GWP and cost was calculated as:

$$\text{GWP}_{\text{total}} = \sum \text{GWP}_i \cdot Q_i \quad (1)$$

$$\text{Cost}_{\text{Total}} = \sum \text{Cost}_i \cdot Q_i \quad (2)$$

Where GWP<sub>i</sub> and Cost<sub>i</sub> represent the unit GWP and cost for an ingredient, Q<sub>i</sub> represents the quantity of an ingredient in a mix.

**Table 4**  
GWP and unit cost inventory of all materials.

Materials	Unit	GWP (kg CO <sub>2</sub> -eq)	Source	Cost (\$AUD)	Source
OPC	kg	0.919	[64,65]	0.2	[66]
RGP	kg	0.0958	[67]	0.11	[68]
FA	kg	0	[64]	0.11	[66]
GGBS	kg	0.190	[64,69]	0.2	[70]
Metasilicate	kg	1.62	[64]	0.4	[71]
NS	kg	4.95E-3	[64]	0.05	[65,66]
RGA	kg	9.4E-3	[72]	0.078	[73]
GO	g	0.046	[74]	33	[75]
SP	kg	4.61	[64]	2.9	[66]
Tap water	kg	4.21E-4	[64]	0.005	[66]

## 4. Experimental results

### 4.1. Engineering properties

Fig. 4a shows the flow table results of cementitious and geopolymer mortars, where the incorporation of RGA, RGP and GO had the same influence on the flowability behaviour in two systems. It can be seen that replacing NS by RGA reduced the workability of fresh mortars in both systems. There was a minimal reduction in flowability when 40 wt% OPC was replaced by RGP. Meanwhile, the workability in geopolymer mortars exhibited a considerable reduction in flowability with the replacement of 40 wt% (FA + GGBS) by RGP. With the addition of 0.1 wt% GO, flowability reduced by 30 % in cementitious mortar whereas reduced only 7 % in geopolymer mortars. As compared between G-GGP and G-GGPGO samples, the addition of 0.1 wt% GO resulted in only a slight 7 % decrease in flowability, which was already low due to the presence of RGP in both mixes. Generally, under the same W/B and A/B ratios, cementitious mortars exhibited higher flowability than geopolymer mortars.

Fig. 4b showed the 28-day compressive strength for cementitious and geopolymer mortars. Replacing NS by RGA reduced the strength by 23 % and 12 % in cementitious mortars and geopolymer mortars respectively. Substituting 40 wt% OPC by RGP reduced 28-day compressive strength by 21 % in cementitious mortars, indicating that the dilution effect of cement outweighed the pozzolanic activity of RGP. Similarly, substituting 40 wt% (FA + GGBS) by RGP reduced 28-day compressive strength by 18 % in geopolymer mortars. With the addition of 0.1 wt% GO, opposite effect on strength was observed in these two systems, 17 % strength reduction in cementitious system and 13 % strength increase in geopolymer system.

Fig. 5 shows the ASR expansion up to 14 days in cementitious and geopolymer mortars respectively when subjected to 80°C 1 N NaOH solution. As expected, excessive expansion was observed in cementitious mortar when natural sand was fully replaced by recycled glass aggregate due to the large amount of amorphous silica in glass, reaching nearly 0.5 % at 14 days which is 5 times higher than the deleterious expansion limit (0.1 %) according to ASTM C 1260 [55]. Minimal expansion was observed within the first 4 days as the silica dissolution from glass was slow under the attack of hydroxyl ions at the early age [33]. When substituting 40 % cement by RGP, ASR expansion caused by glass aggregate was successfully suppressed, which was 0.04 % at 14 days. No

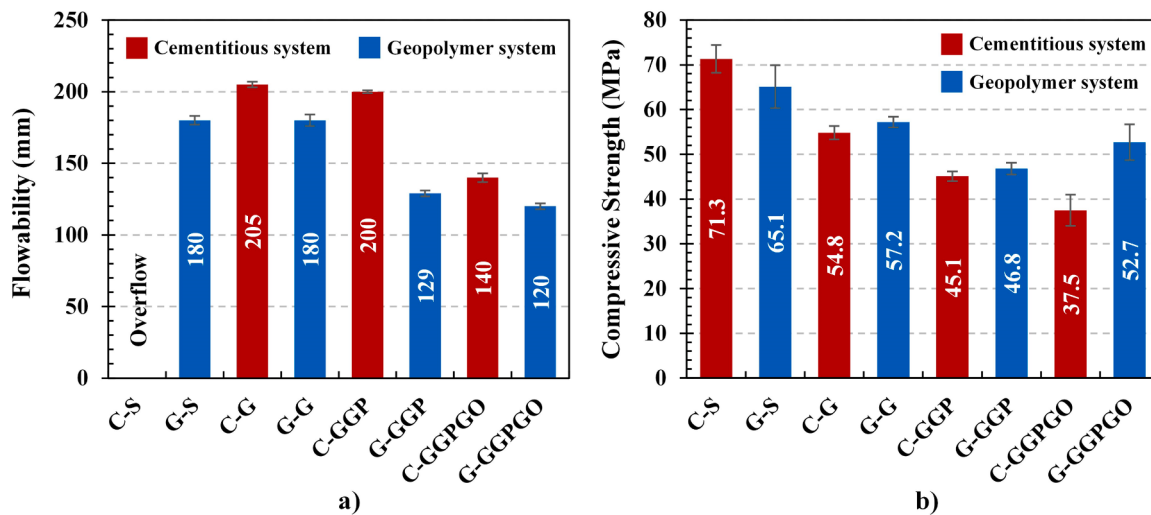


Fig. 4. Effects of RGA, RGP and combined RGP/GO on fresh and hardened properties of cementitious and geopolymer mortars: a) Flowability and b) 28-day compressive strength.

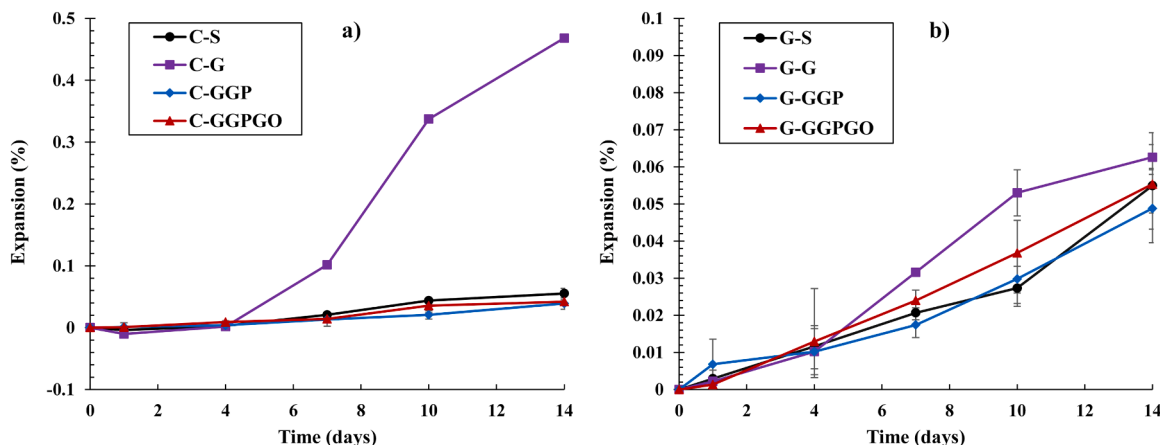
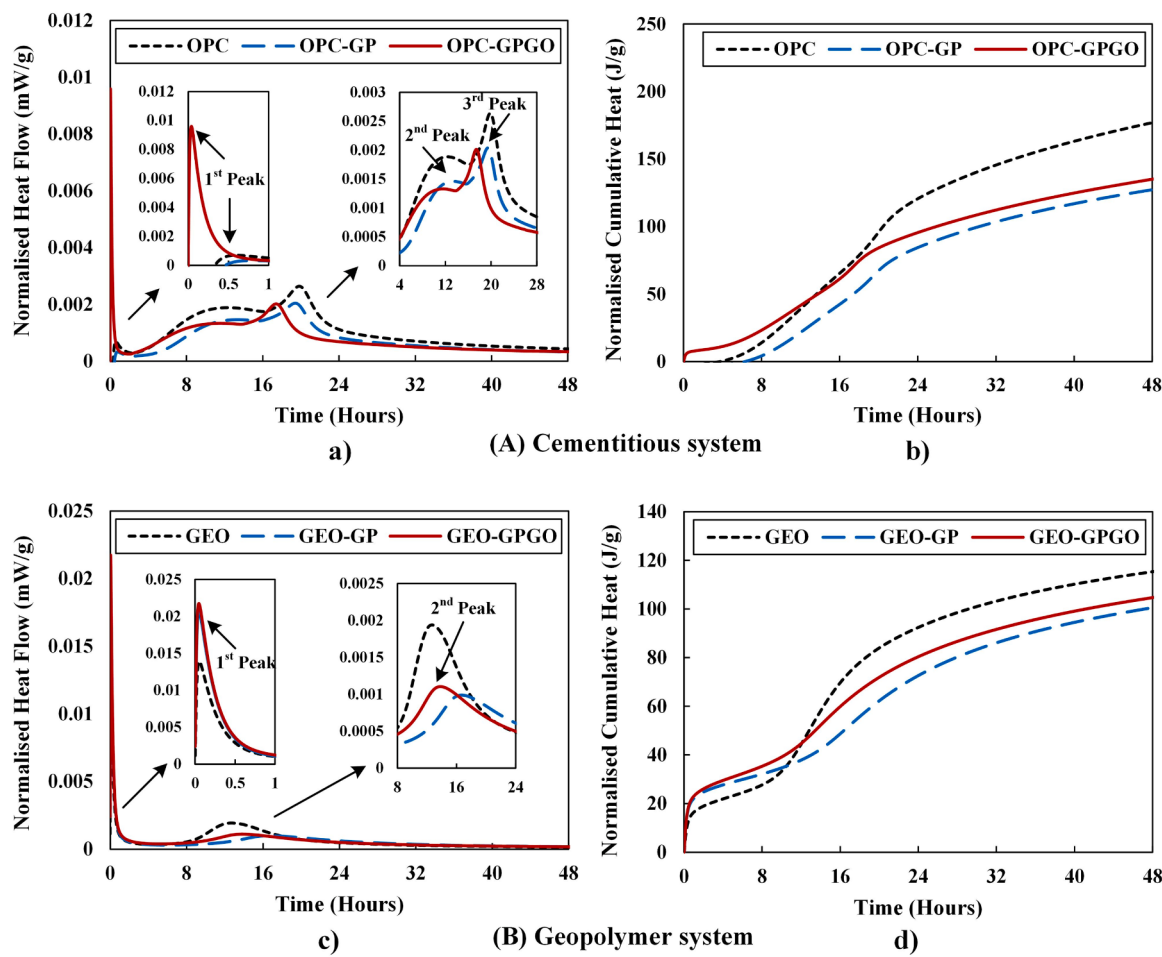


Fig. 5. Effects of RGA, RGP and combined RGP/GO on ASR expansion: a) cementitious materials and b) geopolymer mortars.

change was observed in ASR expansion behaviour of cementitious mortar with the addition of 0.1 wt% GO, suggesting that 40 wt% RGP substitution is effective enough to suppress ASR. On the contrary, despite its high alkali concentration, geopolymer mortars showed much lower expansion incorporating 100 % RGA, reaching 0.06 % at 14 days compared to 0.5 % in cementitious mortars. Similar observation was also reported by previous studies [25,76,77]. The substitution of 40 wt% of FA and GBS with RGP reduced the ASR expansion by 20 % at 14 days. The addition of 0.1 wt% GO in G-GGPGO geopolymer did not show significant change in ASR expansion, suggesting that the current geopolymer system with RGP was effective enough to suppress ASR. Notably, it is common to observe high variation among samples at the early stage of this accelerated test typically due to non-uniform formation of the expansive ASR gel and measurement sensitivity for minimal expansion. The variation was especially notable for geopolymer system observed in Fig. 5b due to a small scale of expansion (below 0.1 %). It is worth noting that the scale of y-axis in Fig. 5a and Fig. 5b is 5 times different to facilitate clearer observation of the minor variations within geopolymer sample group. As the reaction progresses, these variances often become less pronounced, leading to more consistent results in the later stages of the test. Hence, the expansion proportion at 14 days is often used as the key indicator, with an acceptable variance of less than 15 % from the mean value for individual expansion measurements [55].

#### 4.2. Exothermic heat evolution

Fig. 6a shows the early hydration development of cementitious paste up to 2 days. It is apparent that all cementitious groups have the similar evolution of early hydration release, which contains five phases including induction phase, dormant phase, accelerating phase, reduction phase and long-term hydration phase [78]. The 1st peak is due to initial rapid hydration activity when water is added. The 2nd peak is related to the hydration of  $\text{C}_3\text{S}$ , and the 3rd peak corresponds to conversion of ettringite to mono-sulphate [79,80]. It was observed that the OPC-GPGO exhibited a significant increase in the initial reaction heat flow of cementitious materials, indicating that GO accelerated hydration rate on cementitious system, which had a similar effect as other nano-materials such as nano silica or micro silica [81]. The occurrence of heat flow peak during induction phase for OPC-GPGO samples was just 0.04 h, which was earlier than the OPC (0.6 h) and the OPC-GP (0.8 h). Thus, the cumulative heat of GO groups was quite higher than other groups during initial hydration stage. However, the OPC showed the highest heat flow peaks later, as observed from the second and third peaks, and the cumulative heat was thus also higher than other groups. Due to the presence of RGP replacing 40 wt% OPC in both OPC-GP and OPC-GPGO samples, the pozzolanic behaviour of RGP occurred in the later curing phase rather than early hydration stage. The third peak of heat flow was assigned to the consumption of gypsum and the



**Fig. 6.** Isothermal calorimetry results showing the effects of RGP and combined RGP/GO: (a – b) normalised heat flow and cumulative heat of cementitious pastes; (c – d) normalised heat flow and cumulative heat of geopolymer pastes.

generation of ettringite [82], and that peak in OPC-GPGO sample appeared at 17.4 h, approx. 2 h earlier than the OPC (19.8 h) and OPC-GP samples (19.4 h), indicating that the incorporation of GO significantly accelerated the hydration of C<sub>3</sub>A [83]. As shown in Fig. 6b, the cumulative heat of OPC samples (176.6 J/g) was higher than OPC-GP (127.2 J/g) and OPC-GPGO samples (134.8 J/g) at 48 h. Apparently, the replacement of cement by RGP slowed down the hydration mainly due to the dilution effect [84].

Unlike cementitious system, geopolymer system exhibited only two major peaks. The precursors substitution by RGP tended to accelerate the initial dissolution in the induction phase at a very first hour of reaction, as shown in Fig. 6c. This phenomenon was even pronounced with the inclusion of GO in the GEO-GPGO mixtures. However, RGP also exhibited the retarding effect on geopolymserisation as the main reaction of GEO-GP mixes reached its second exothermic peak at 16.7 hours, compared to 12.7 hours of the control GEO mixes. In comparison to that of GEO-GP mixes, the inclusion of GO in GEO-GPGO mixes promoted the main reaction (peaked at 13.8 hours of reaction) and intensity of second reaction peak. The cumulative heat evolutions of GEO-GP and GEO-GPGO mixtures were only higher than the control GEO mixes within the first 12 hours of reaction as shown in Fig. 6d. When the geopolymserisation process kept proceeding, the GEO-GP and GEO-GPGO mixtures showed lower cumulative reaction heat, which obtained 100.5 J/g and 104.8 J/g respectively, compared to that of the control (115.5 J/g) after the same 48-hour reaction.

#### 4.3. XRD diffractograms

For cementitious paste, the detected mineral phases included portlandite (PDF 00–044–1481), calcite (CaCO<sub>3</sub>) (PDF 00–005–0586), ettringite (PDF 04–013–3691), gypsum (PDF 00–033–0311), C-S-H, alite (C<sub>3</sub>S) (PDF 00–049–0442) and belite (C<sub>2</sub>S) (PDF 00–033–0302), as shown in Fig. 7a. The peak intensity of ettringite is closely related to the hydration of C<sub>3</sub>A and gypsum, and the peak intensity of C-S-H gels and portlandite is dominated by the hydration of C<sub>2</sub>S and C<sub>3</sub>S and the pozzolanic reaction of RGP. The carbonation of portlandite affects the peak intensity of calcite. Compared with control OPC mixes, a lower peak intensity was found for C<sub>2</sub>S, C<sub>3</sub>S and gypsum in both OPC-GP and OPC-GPGO mixes due to the dilution effect when substituting 40 wt% OPC with RGP. The presence of C<sub>2</sub>S and C<sub>3</sub>S phases at 28 days across all mixes indicates incomplete hydration under ambient curing condition, which explains the decrease in compressive strength and the variations in heat of hydration. A reduced peak intensity for portlandite ( $\theta = 18^\circ$ ,  $29^\circ$ ,  $33^\circ$ ,  $34^\circ$ , and  $47^\circ$ ) was also observed in OPC-GP mixes. Further reduction in the peak intensity for portlandite was observed in OPC-GPGO mixes as the addition of 0.1 wt% GO promoted the cement hydration and pozzolanic reaction of RGP, which also led to a wider amorphous hump of C-S-H at  $29.4^\circ$   $\theta$  [85]. Moreover, there was no obvious difference in the diffraction peaks of the hydration products of OPC-GPGO mixes, indicating that adding 0.1 wt% GO did not change the crystal structure of the hydration products, and did not induce the formation of new hydration products. Nonetheless, the peak intensity of calcite ( $\theta = 29.5^\circ$ ) OPC-GPGO exhibited an increase, indicating that the GO promoted the carbonation process [85].

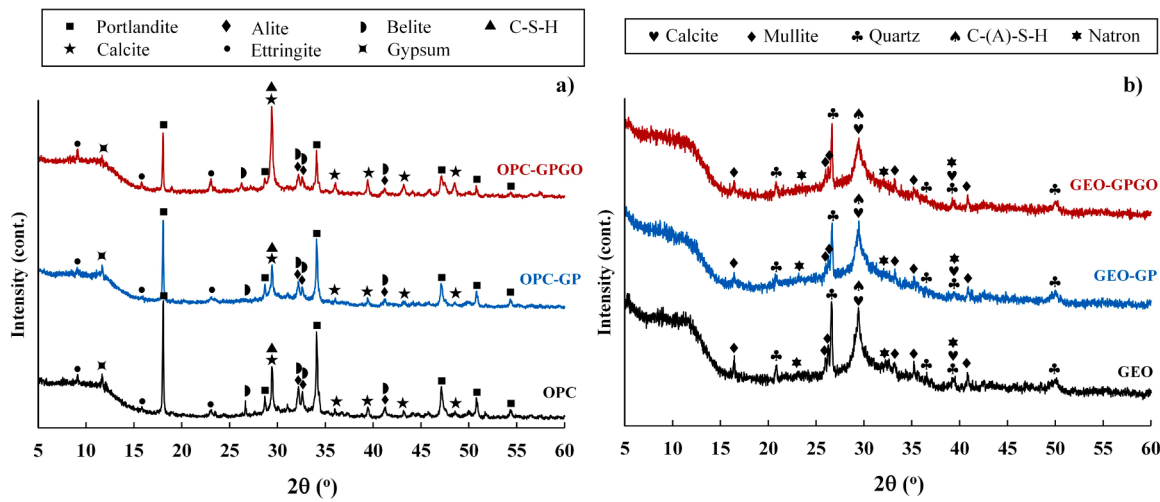


**Fig. 7.** XRD diffractograms showing the effects of RGP and combined RGP/GO on hydration and geopolymerisation at 28 days: a) cementitious system, b) geopolymer system.

For geopolymer system, the four main phases were detected including quartz (PDF 01-078-1252), mullite (PDF 01-083-1881), calcite (PDF 01-083-4601), natron (PDF 00-015-0800) and calcium (alumino)silicate hydrate (C-(A)-S-H) gels. The diffraction pattern positioned around  $29.5^\circ$   $2\theta$  was associated with both C-(A)-S-H gels characterised by amorphous hump (i.e., broad peak) and crystalline calcite phases featured by sharp peak. The C-(A)-S-H hump was broadened when replacing precursors by RGP as observed in both GEO-GP and GEO-GPGO mixes, indicating an increased amorphous gel content. However, their intensities at this diffuse band seemed to be lower than the control GEO, which implied lesser C-(A)-S-H gels in these two modified mixes and thus resulted in lower compressive strength than the control GEO mixes, as shown in Fig. 4b. It should be noted that GEO-GPGO mixes seemed to exhibit a low amount of calcite phases than other mixes, as the sharp peak tip was diminished corresponding to the addition of GO. Also, amorphous C-(A)-S-H hump in GEO-GPGO mixes was found to be broader than that in GEO-GP mixes, with more gel formation. The characteristic peaks of quartz (e.g.,  $20.8^\circ$  and  $26.6^\circ$   $2\theta$ ) and mullite phases (e.g.,  $16.5^\circ$ ,  $26^\circ$  and  $26.3^\circ$   $2\theta$ ) for GEO-GP and GEO-GPGO mixes exhibit reduced intensities compared to that for the control GEO. This phenomenon mainly related to the replacement of FA/GGBS precursors by RGP.

#### 4.4. FTIR spectra

Fig. 8a shows the FTIR results for the cementitious pastes modified by RGP and GO. The wavenumber range of  $3700 - 3200 \text{ cm}^{-1}$  can be

attributed to the O-H stretching vibration in cementitious matrix, corresponding to the structural water molecules within C-S-H gels. The FTIR wavenumber peak around  $1640 \text{ cm}^{-1}$  also characterises the bending vibration of H-O-H bonds of free and adsorbed water [86]. The increased formation of C-S-H gels is associated with the effective interaction between GO and the cementitious matrix, which facilitates the incorporation of additional water into the gel structure. Thus, the broad absorption of shoulder bands with the inclusion of 0.1 wt% GO suggests an increase in structural water within the C-S-H gels in the cementitious matrix. This is consistent with the XRD results (see Fig. 7a), which show a greater presence of C-S-H corresponding to the addition of GO. The wavenumber within  $1470 - 1400 \text{ cm}^{-1}$  and  $875 \text{ cm}^{-1}$  corresponds to the presence of  $\text{CaCO}_3$  due to carbonation process. Interestingly, there was a significant increase in the intensity of these bands, demonstrating that the OPC-GPGO mixes with GO inclusion had substantially higher calcium carbonate products than other cementitious mixes, which was also found in XRD results as shown in see Fig. 7a. Minor peaks at  $1150 - 1100 \text{ cm}^{-1}$  and  $690 - 600 \text{ cm}^{-1}$  were attributed to the  $\text{SO}_4^{2-}$  groups from gypsum or ettringite phases. The absorption band at  $1100 - 900 \text{ cm}^{-1}$  and  $500 - 400 \text{ cm}^{-1}$  were indicative of the vibrations of Si-O and O-Si-O bonds, reflecting the presence of C-S-H phase [87]. The intensity of these bands was significantly pronounced for OPC-GPGO samples, demonstrating that the presence of GO promoted the formation of C-S-H gels. Specifically, the oxygen-containing functional groups on the GO surface can provide nucleation sites for the increasing formation of C-S-H gels [88].

For the geopolymer system, the result exhibited no significant

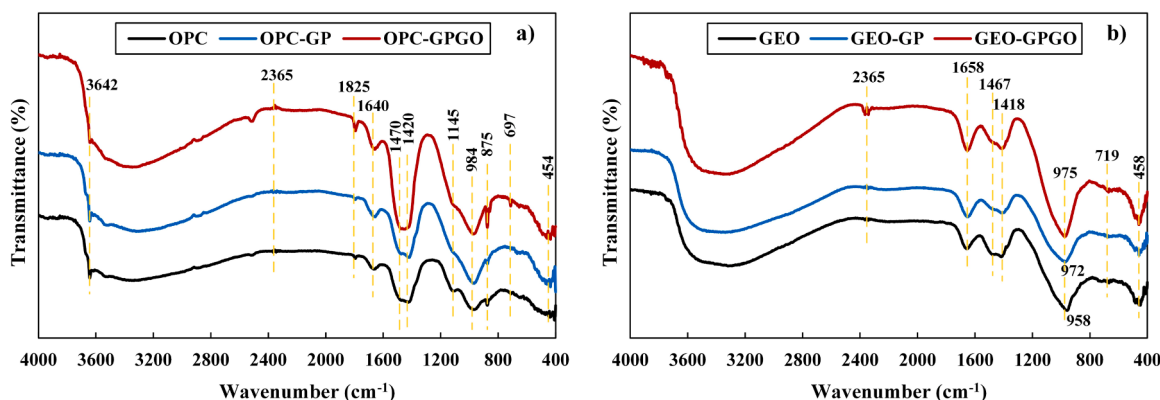


**Fig. 8.** FTIR spectra displaying the effects of RGP and combined RGP/GO on hydration and geopolymerisation: a) cementitious system, b) geopolymer system.

distinct in FTIR spectra among geopolymer mixes, except for their transmittance intensity at several wavenumbers. The shoulder spreading within  $3650 - 2800 \text{ cm}^{-1}$  was indicative of the O-H stretching vibration; meanwhile, the weak band at around  $1658 \text{ cm}^{-1}$  was assigned to the H-O-H bending of physically bound water in silanol groups [89,90]. Especially, only GEO-GPGO mixes showed the peak at approx.  $2365 \text{ cm}^{-1}$ , which represented the C-O-C stretching vibration of GO [91] and polycarboxylate-ethers-based SP, which contain ether linkages. The O-C-O and C=O bonds were detected at the wavenumber of  $1467 \text{ cm}^{-1}$  and  $1418 \text{ cm}^{-1}$  respectively, suggesting the presence of carbonate groups (i.e.,  $\text{CO}_3^{2-}$ ) in the mixes formed through the reaction between alkali metal hydroxide and atmospheric  $\text{CO}_2$  [92,93]. The asymmetric stretching Si-O, Si-O-Si and Si-O-Al bonds appeared at around  $958 - 975 \text{ cm}^{-1}$ , implying the binding structure of amorphous aluminosilicate gel phases [89,94]. The lower wavenumber of this band within  $950 - 1100 \text{ cm}^{-1}$  is indicative of a reduced degree of cross-linking within the amorphous phase as observed for all geopolymer mixes, attributed to the increased calcium content in the gel structure [95]. As observed, the shift of the Si-O-T bands ( $T = \text{Si}, \text{Al}$ ) from  $958 \text{ cm}^{-1}$  to  $972 \text{ cm}^{-1}$  and  $975 \text{ cm}^{-1}$  when introducing RGP and GO revealed a denser aluminosilicate network with higher Si/Al ratio. Moreover, the sharpness of this absorption band correlates with the concentration of tetrahedrally coordinated aluminum in the geopolymer matrices, signifying a degree of geopolymerisation [89]. The GEO-GPGO samples exhibited higher intensities in this Si-O-T band at  $975 \text{ cm}^{-1}$  than other samples, indicating the higher reaction rate with an increased gel formation. The absorption bands observed at approx.  $719 \text{ cm}^{-1}$  and  $458 \text{ cm}^{-1}$  corresponded to the stretching and bending vibrations of Si-O-Si and O-Si-O bonds in the  $\text{SiO}_4$  tetrahedral groups, similar to that of symmetrical stretching vibrations of Al-O bonds in Si-O-Al linkages [96,97].

#### 4.5. TG/DTG analysis

Fig. 9a shows TG/DTG results for cementitious systems where all three mixes showed similar weight loss patterns. Three stages of weight loss bands were observed: Phase I (0–200 °C) characterises the dehydration mass loss zone of C-S-H gels and hydrated calcium aluminate (Afm), Phase II (400–500 °C) is the zone of portlandite dehydroxylation, and Phase III (600–800 °C) is the zone of decomposition calcite ( $\text{CaCO}_3$ ) [98]. In comparison with control OPC mixes, lower peak intensity of Phase I and Phase II were found in OPC-GP and OPC-GPGO mixes, indicating that there was less amount of bound water and portlandite. Additionally, there was a higher amount of  $\text{CaCO}_3$  in OPC-GPGO mixes and lower amount of portlandite, which was consistent with the XRD results as mentioned in Section 4.3 and Section 4.4.

As observed from TG/DTG in Fig. 9b, the mass loss of geopolymer

samples took place under three main phases, including the major evaporation of physically bound water (< 230 °C), volatilisation of chemically bound water, dehydroxylation of hydroxyl groups and partly decomposition of C-(A)-S-H gels (230–700 °C), decomposition of calcite and other phases (> 700 °C) [34,99]. From the TG curve, the major mass loss triggered by free water evaporation and dehydration of Natron [100] occurred at low temperature for GEO-GP samples (67.5 °C), followed by GEO-GPGO (57.4 °C) and GEO samples (61.7 °C). The shallow shoulder observed around 360 °C was attributed to the release of interlayer water from geopolymeric gels. This also reflected a higher geopolymerisation degree of the control GEO in comparison to that of GEO-GP and GEO-GPGO mixes when replacing precursor by high volume RGP (40 %) in both latter mixes. The peak observed around 700 °C was associated with the decarbonation of calcite. Evidently, the control GEO mixes had higher amount of calcite and thus exhibited higher intensity of decarbonation, which shared a similar observation to XRD results as in Fig. 7b. Exposing to above 700 °C led to the loss of binding water in C-A-S-H gels and the transformation into crystalline phases (e.g., wollastonite, gehlenite) from the disrupted gel structure [34]. From the DTG curve, the control GEO mixes exhibited less mass loss than the GEO-GP and GEO-GPGO mixes below 400 °C, but this trend reserved when the exposure temperature increased to 800 °C.

#### 4.6. SEM/EDS characterisation

Fig. 10a illustrates the microstructure of cementitious mortars, highlighting the effects of RGA, RGP and GO. The microstructures of C-S and C-G mortar mixes were relatively similar, with noticeable differences only in ITZ between aggregate and matrix. Although both types of aggregates demonstrated poor bonding with the matrix, RGA exhibited slightly better interfacial characteristic with cementitious matrix than sand. When 40 wt% of OPC was replaced by RGP, the interfacial characteristics exhibited negligible changes. The inclusion of 0.1 wt% GO in C-GGPGO resulted in densification of both the matrix and the matrix-aggregate interface.

The SEM micrographs for geopolymer mortar are displayed in Fig. 10b. There was an interfacial gap between geopolymer matrix and aggregate (either NS or RGA) without significant differences in their microstructure. Smooth surface of RGA seemed to have poorer interfacial bonding with matrix in comparison to the rough surface of NS. The control one-part geopolymer matrix using FA and GGBS exhibited voids and multiple micro-cracks in the microstructure. These defects were caused by water evaporation and drying shrinkage, which could be ascribed to a high calcium content in the mixes [101]. When replacing precursors by RGP, the microstructure appeared to achieve better homogeneity. This effect was more pronounced with the inclusion of 0.1 wt% GO to further densify the microstructure and interfacial

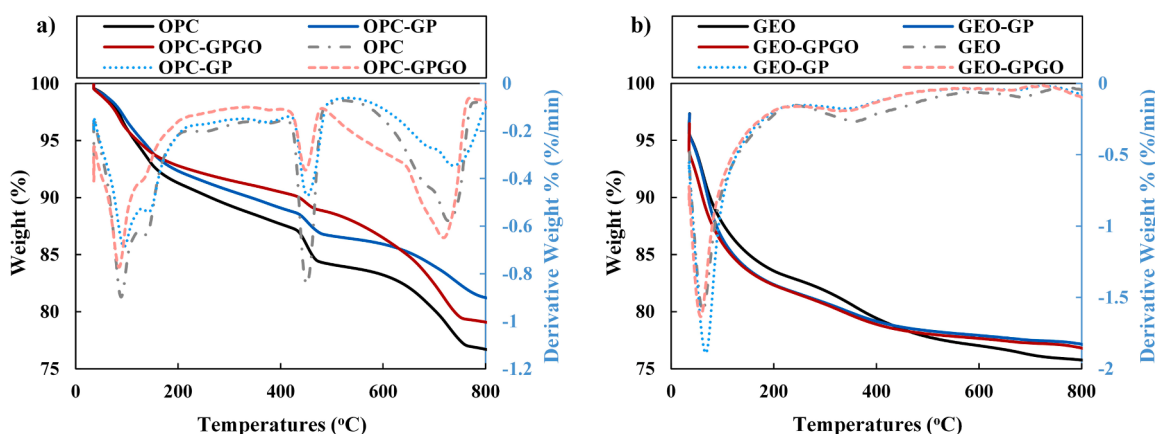
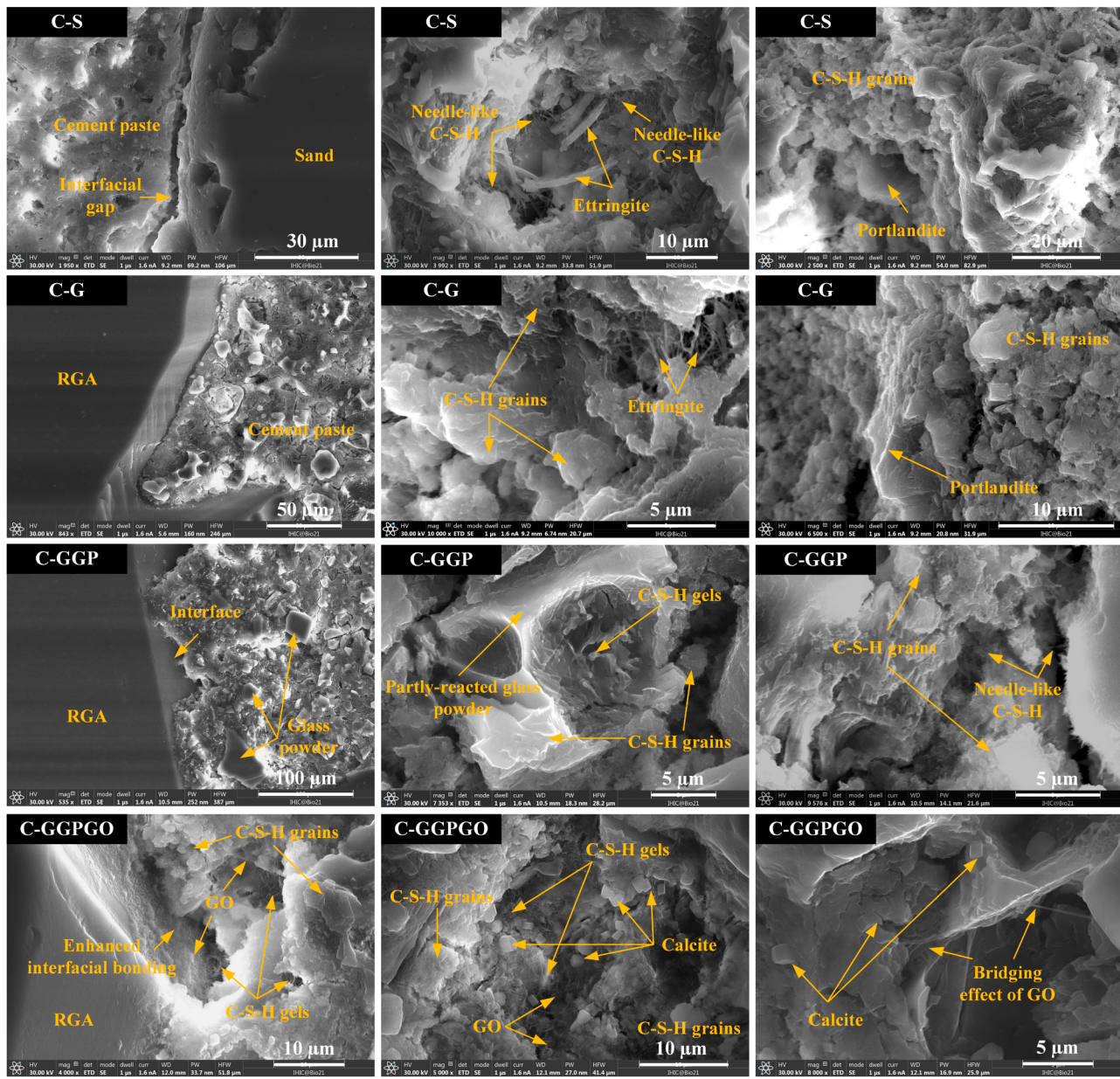


Fig. 9. TG/DTG curves reflecting the effects of RGP and combined RGP/GO on hydration and geopolymerisation: a) cementitious system, b) geopolymer system.



(A) Cementitious system

Fig. 10. SEM micrographs reflecting microstructure of (A) cementitious system and (B) geopolymer systems with different inclusion of RGA, RGP and GO.,,

matrix-aggregate zone as seen in G-GGPGO samples.

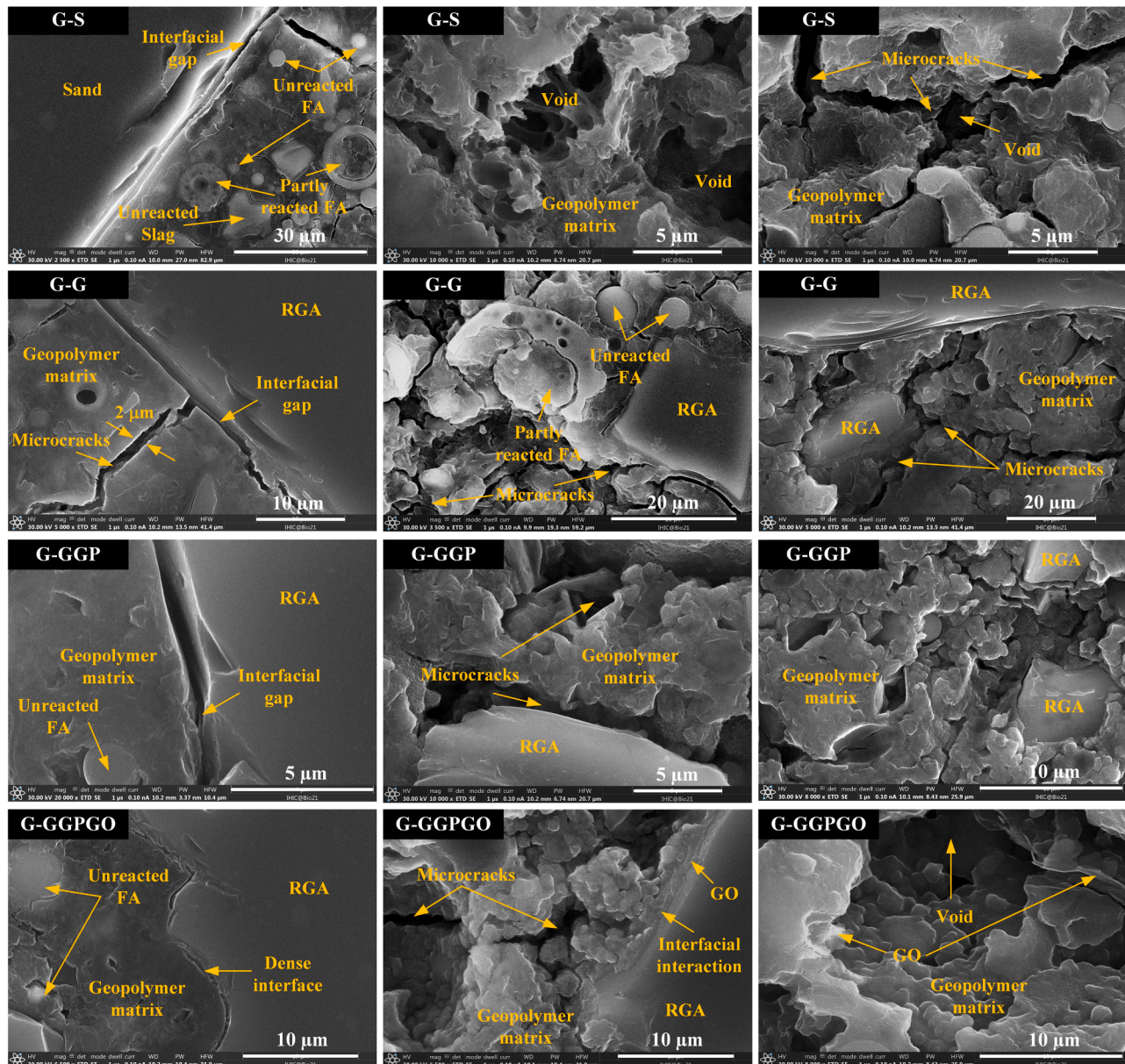
The interfacial transition zone (ITZ) thickness was measured using EDS line analysis to determine the effects of RGA, RGP and GO on microstructural densification, as depicted in Fig. 11. In cementitious system, the matrix-aggregate ITZ thickness was approximately 30 µm for NS and 20 µm for RGA. In the C-GGP samples, replacing OPC with RGP did not improve the ITZ, instead slightly increasing its thickness. However, the addition of GO reduced the ITZ thickness to approx. 10 µm, indicating a significantly denser microstructure. For geopolymer system, the ITZ thickness between geopolymer and aggregate (either sand or RGA) seemed relatively narrow and similar at around 5 µm. With the incorporation of RGP as precursor substitution, the geopolymer-RGA ITZ thickness gradually reduced to approx. 2 µm as measured the average. The denser ITZ between geopolymer and RGA (1 µm) was observed in G-GGPGO with 0.1 % of GO, corroborating the observation from SEM. Overall, geopolymer matrices had narrower ITZ thickness with

aggregate than cementitious matrices.

## 5. Discussion

### 5.1. Effects of RGA

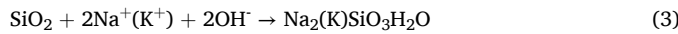
As the particle size distribution was the same for NS and RGA in this study, the observed workability reduction (see Fig. 4a) can be attributed to the sharper edges, more angular shape, and harsher texture of RGA compared to NS, which hinder the movement of cement/geopolymer paste surrounding the glass particles [9,102,103]. Regarding ASR, under high pH value of alkali, the OH<sup>-</sup> (often due to the presence of portlandite) in pore solution tended to move towards the interfacial zones of RGA, and Na<sup>+</sup> or K<sup>+</sup> or Ca<sup>2+</sup> could also quickly diffuse to the interface areas of RGA. This leads to the depolymerisation of silicate (amorphous SiO<sub>2</sub> of RGA), ultimately forming the ASR swelling gels (Na<sub>2</sub>(K)



(B) Geopolymer system

Fig. 10. (continued).

$\text{SiO}_3\text{H}_2\text{O}$ ) [104], as expressed by Eq. (3). This expansive phenomenon could induce internal stress and cracking and thus diminished strength characteristics of matrix.



The study identified significant ASR expansion in the C-G samples (refer to Fig. 5a). In common, ASR phenomena predominantly occur inside RGA, rather than on the surfaces of RGA. However, internal cracks of the RGA enable ASR gels to fill these expansion cracks at the interface zones between RGA and the cementitious matrix [105–107]. Due to the ambient curing condition employed in this study, the mortar might experience shrinkage caused by water loss [108], leading to numerous micro-cracks networks throughout the matrix. Consequently, the ASR phenomenon primarily manifested on the surface of the RGA. Furthermore, the expansion pressure from the water absorption of ASR gels mainly occurred near the void regions, which might have caused the enlargement and proliferation of micro-cracks in these localised void

areas without damaging the RGA itself. Therefore, the porosity of the matrices could somewhat mitigate the ASR-induced expansion pressure [105]. However, the angular and shape morphology of RGA could serve as potential sites for crack initiation, in contrast to the smoother surface of sand, consequently diminishing the overall strength of the matrix as observed in the C-G groups as shown in Fig. 4b. It was observed in Fig. 5b that the geopolymer matrix demonstrated lower susceptibility to ASR compared to the cementitious matrix. The main reason could be the low calcium content in the geopolymer system, which produced less expansive ASR gel compared to the expansive calcium rich ASR gel in cementitious system [109,110]. The CaO content in RGP (9.53 %) is much lower than that in GGBS (44.34 %) (see Table 1), leading to a reduced formation of portlandite ( $\text{Ca}(\text{OH})_2$ ) – a major source of  $\text{OH}^-$  in the whole system, for ASR. Another possible reason could be the higher number of micro-cracks and pores in geopolymer mortars which can accommodate more ASR gels to mitigate expansion-induced stress [25, 111]. Also, the absence of portlandite, the incorporation of alkali ions

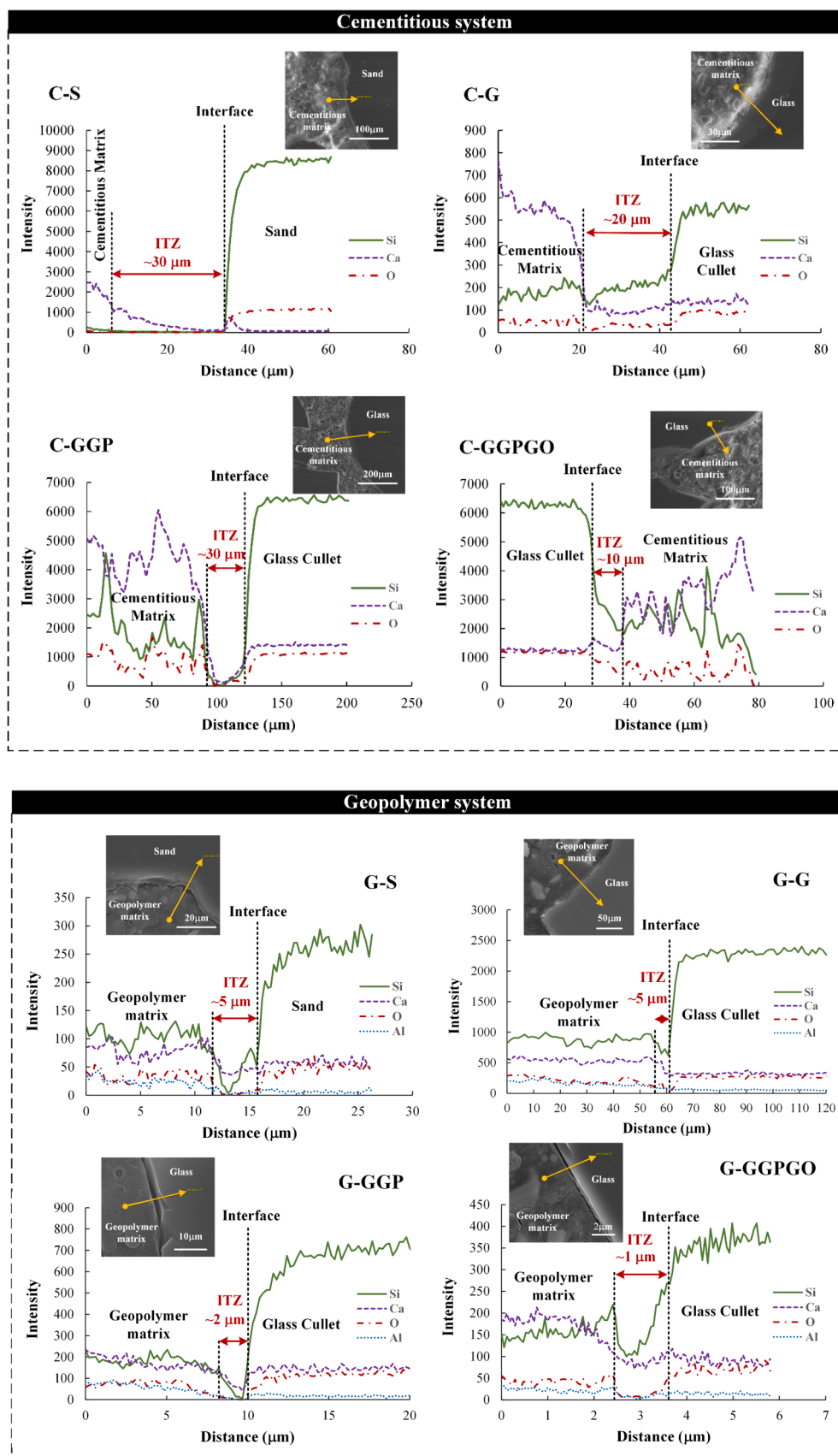
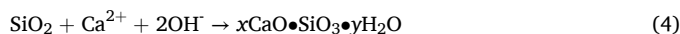


Fig. 11. EDS line analysis of matrix-aggregate interface in both cementitious and geopolymer systems with different inclusion of RGA, RGP and GO.

into N-A-S-H gels to reduce the availability of free alkalis, higher alkali binding capacity, and denser microstructure of geopolymer matrices compared to cementitious system (proved by SEM/EDS in Fig. 10 and Fig. 11), which limited the movement of water and alkali ions. The ASR reaction mechanism for both cementitious and geopolymer system is depicted in Fig. 12.

## 5.2. Effects of RGP

When replacing binders by RGP, the cementitious mixture still achieved comparable workability, which could be attributed to the counteraction between the negative effects induced by larger surface area and the positive effects induced by smoother surface of RGP compared to cement [18]. However, the negative effects induced by the less spherical particle shape of RGP compared to FA [112] and more finer particles than GGBS significantly reduced the flowability of geopolymer mixture (see Fig. 4a). Besides, the incorporation of a high amount of RGP decreases the amount of tricalcium silicate ( $C_3S$ ) and dicalcium silicate ( $C_2S$ ) in the mixture, leading to a reduced formation of C-S-H gels in the matrix compared to the control. Due to the prolonged duration of the pozzolanic reaction, partially reacted RGP was still present throughout the matrix at 28 days, leading to heterogeneity (see Fig. 10) and somewhat impacting the matrix's strength (see Fig. 4b). Also, RGP mitigated ASR in cementitious matrix through several mechanisms, including the pozzolanic reaction, dilution effects and carbonation [113, 114]. The amorphous silica in RGP interacted with portlandite via pozzolanic reaction, forming secondary C-S-H gel, as shown in Eq. (4). This process not only enhances the microstructure but also reduces the amount of reactive silica available in pore solution for ASR. By diluting the OPC content by RGP, the overall pH and alkali content of reactive components (i.e., hydroxyl ion ( $OH^-$ ) concentration) in the pore solution decreased. This effects of RGP, in turn, significantly mitigated the ASR expansion in cementitious matrices containing RGA.



The carbonation process also contributed to the ASR mitigation. The evaporation of water under ambient curing conditions somewhat triggered increased cracking and porosity, thereby facilitating the diffusion of  $CO_2$ , leading to significant carbonation reaction within the matrices (see Fig. 7). This effect together with pozzolanic reaction resulted in a significant reduction in portlandite phase in matrix (according to XRD and TGA results, see Fig. 7 and Fig. 9 [115]). Free  $Ca(OH)_2$  is identified as the primary contributor to weak zones within the matrix and acts as a reservoir of alkali ions that facilitate ASR. The incorporation of  $Ca(OH)_2$  into hydration reactions results in its depletion from the cementitious system. In addition, previous research had demonstrated the immobilisation of free alkali metal ions within the C-S-H gel layer [116] and this phenomenon was further pronounced under carbonation through Phase I, II, III [117], as illustrated in Fig. 13. Carbonation reduces the free  $Ca^{2+}$  content in the C-S-H gel layer, resulting in more free alkali metal ions being bound to the C-S-H gel to maintain charge balance. This binding mechanism of C-S-H gels shares some similarity to that of C-A-S-H in geopolymer system that limit the cations for ASR (Fig. 13). Such mechanism led to fewer free alkali metal ions in the pore solution, thereby mitigating the ASR phenomenon. Also, it explains the relatively low ASR levels observed in the C-GP and C-GPGO groups (see Fig. 5). In addition, the occurrence of ASR requires sufficient active  $SiO_2$  and alkaline metal ions, as well as high pH and sufficient water. The local carbonisation behaviour can reduce the pH value in the matrix and allow more free metal ions to be solidified into C-S-H, and thus the calcite generated by carbonisation process can limit the ingress of water and alkalis. Therefore, the ambient curing can somewhat reduce the ASR behaviour of matrices.

In a geopolymer system, the presence of RGP with high alkalinity (11.5 %  $Na_2O$  – see Table 1) can increase the  $Na^+$  concentration in the pore solution, enhancing the dissolution rate of reactive Si and Al species from the precursors. The broad hump observed in the diffraction pattern of C-A-S-H indicates an increased amorphous content due to the dissolution of RGP and more disordered atomic arrangements (Si, Al, and Ca) within the C-A-S-H network [118]. Larger RGP particles react more

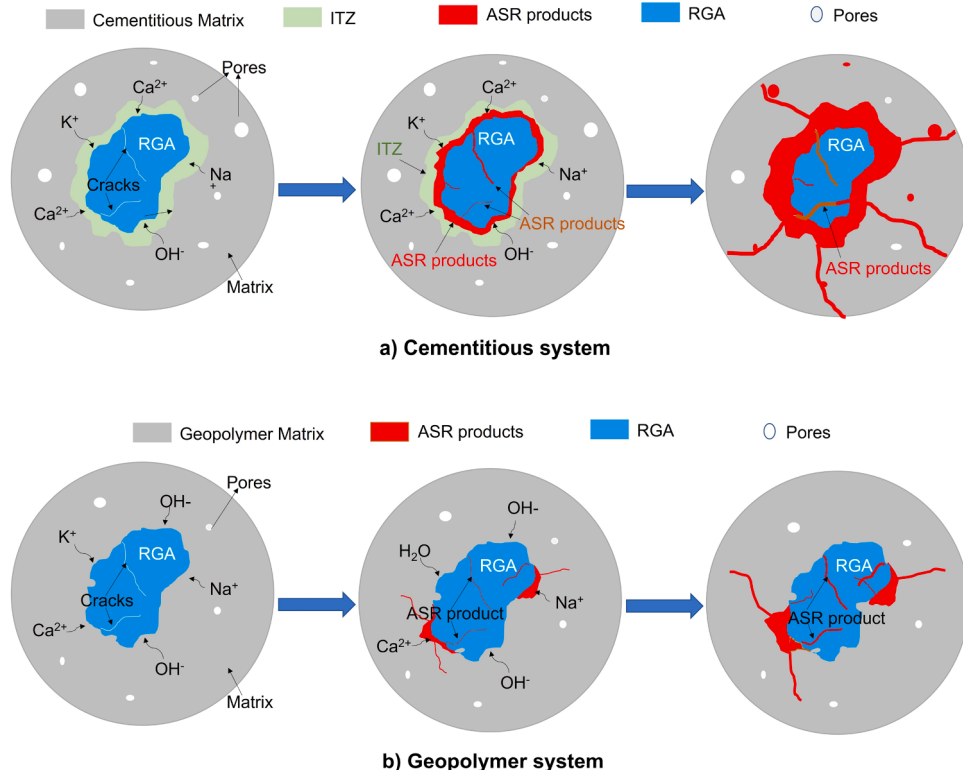


Fig. 12. The ASR mechanisms of RGA in both a) cementitious matrix, b) geopolymer matrix.

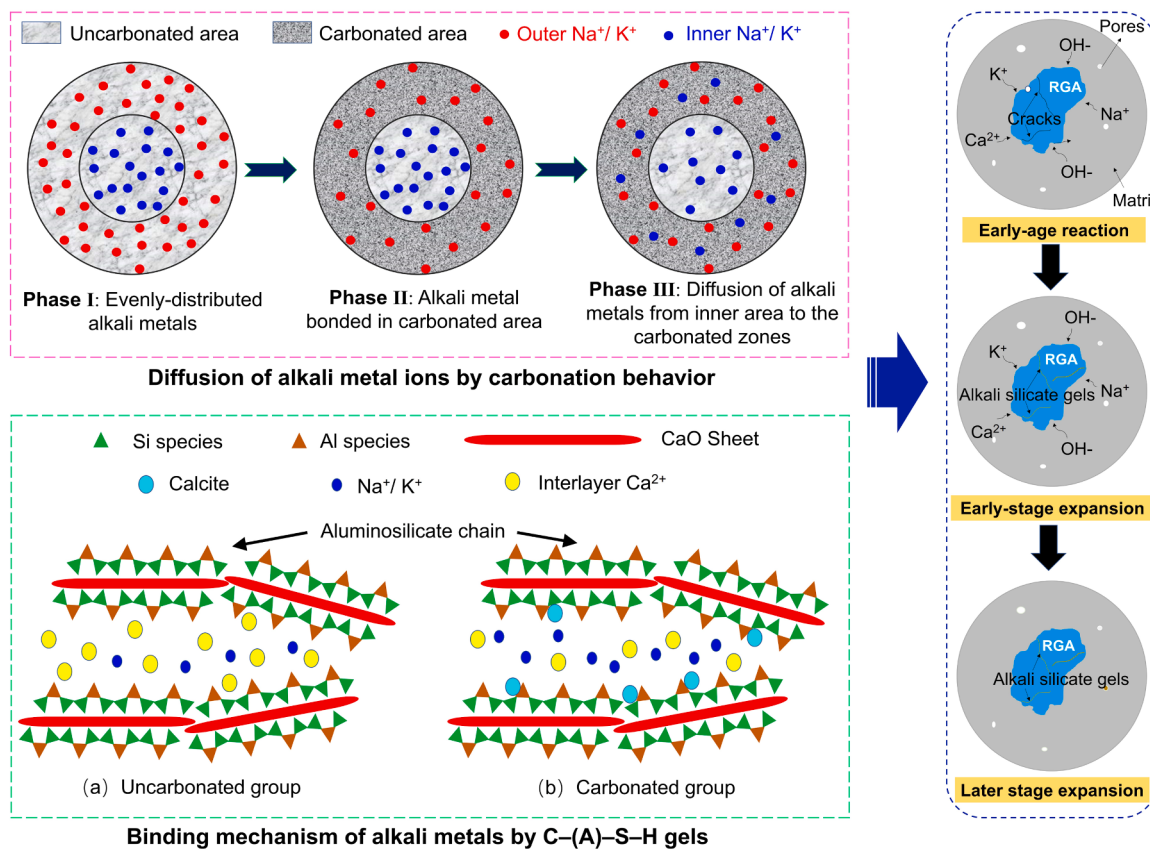


Fig. 13. Alkali binding mechanism of C-(A)-S-H gels suppressing ASR.

slowly (i.e., partly-reacted particles as observed in Fig. 10), resulting in a mixture of amorphous and crystalline phases. The modification of the silicate network (Si-O-Si and Si-O-Al) and hydroxyl groups ( $\text{OH}^-$ ) is evidenced by FTIR corresponding to the increased intensity of absorption bands around  $950\text{--}1200\text{ cm}^{-1}$  and  $3200\text{--}3600\text{ cm}^{-1}$ . However, the deficiency of Al species in RGP limits the formation of Al-O and Al-O-Al linkages, affecting the main reaction and resulting in reduced C-(A)-S-H gel formation and lower compressive strength (see Fig. 4b). This observation shares a similarity to other study in which high intensity peak at  $1650\text{ cm}^{-1}$  and the broad hump  $3300\text{--}3500\text{ cm}^{-1}$  confirm increased silanol groups (Si-OH) for geopolymserisation with the presence of RGP [119]. Regarding ASR mechanism, the amorphous silica from RGP reacts with the alkaline activator during geopolymserisation to form stable geopolymeric gels. Those N-A-S-H gels immobilise alkali ions, thereby reducing the concentration of free alkali ions available to react with silica. Additionally, the geopolymserisation at later stages further refines the pore structure, decreasing permeability and inhibiting the diffusion of alkali ions and water, both of which are essential for the ASR mechanism. Those phenomena contribute to the significant mitigation of the ASR-induced expansion (see Fig. 5b). Overall, the general mechanism of RGP for suppressing ASR in both cementitious and geopolym system share some similarities.

### 5.3. Effects of GO

GO's high specific surface area and functional groups (hydroxyl, carboxyl, epoxy, and carbonyl) facilitate bonding with C-S-H gels via hydrogen bonding, electrostatic interactions, coordination bonds, and van der Waals forces [120]. The large surface area of the hydrophilic GO absorbed water molecules to its surface, which reduced the free water content for lubrication [121,122], and thus led to a significant reduction in flowability (see Fig. 4a). These characteristics of GO also promoted

the dissolution, release, and migration of  $\text{Ca}^{2+}$  from  $\text{C}_3\text{S}/\text{C}_2\text{S}$ , promoting hydration. The presence of GO significantly accelerated hydration process at early age which can be seen from calorimetry results within a very first hour (see Fig. 6a and b). As hydration progresses, GO-modified C-S-H bridges facilitate the movement of  $\text{Ca}^{2+}$  and  $\text{Si}^{4+}$  ions towards areas with high GO concentration [123]. This phenomenon significantly increased C-S-H gel content – confirmed by XRD and FTIR results (see Fig. 7 and Fig. 8) and forming a dense ITZ and matrix that enhanced the microstructure (see Fig. 10 and Fig. 11), thus retarding the diffusion of ions. Despite higher hydration rate and higher formation of C-S-H gels and the densification of the microstructure, the cementitious mortar with GO inclusion (C-GGPGO) exhibited a lower compressive strength than those without GO (C-GGP), as shown in Fig. 4b. This phenomenon was ascribed to the adverse effect of ambient curing in this study. Rapid water consumption without water-curing to supply water for hydration reaction may lead to self-desiccation and shrinkage with major micro-cracks. The shrinkage-induced cracks under drying condition counteracts and worsen the strength development. On the contrary, geopolymmer mortar exhibited a strength improvement with GO addition, which could be attributed to the distinct nature of geopolymserisation and cement hydration processes. GO contributed to the reinforcement and bridging of geopolym chain within the microstructure, as well as necessitated minimal water for the geopolymserisation, thereby increasing compressive strength of geopolym matrices. To clarify the combined effect of materials on microstructure, the mechanism was illustrated in Fig. 14. Functional groups of GO facilitated the better interaction between matrix and the surface of RGA during geopolymserisation.

For ASR in geopolym, N-A-S-H and C-A-S-H gels have capacity to bind higher quantity of alkalis than normal C-S-H gels, further reducing alkali concentration in the pore solution [124]. Furthermore, nucleation seeding effects of GO further accelerated the dissolution and hydration

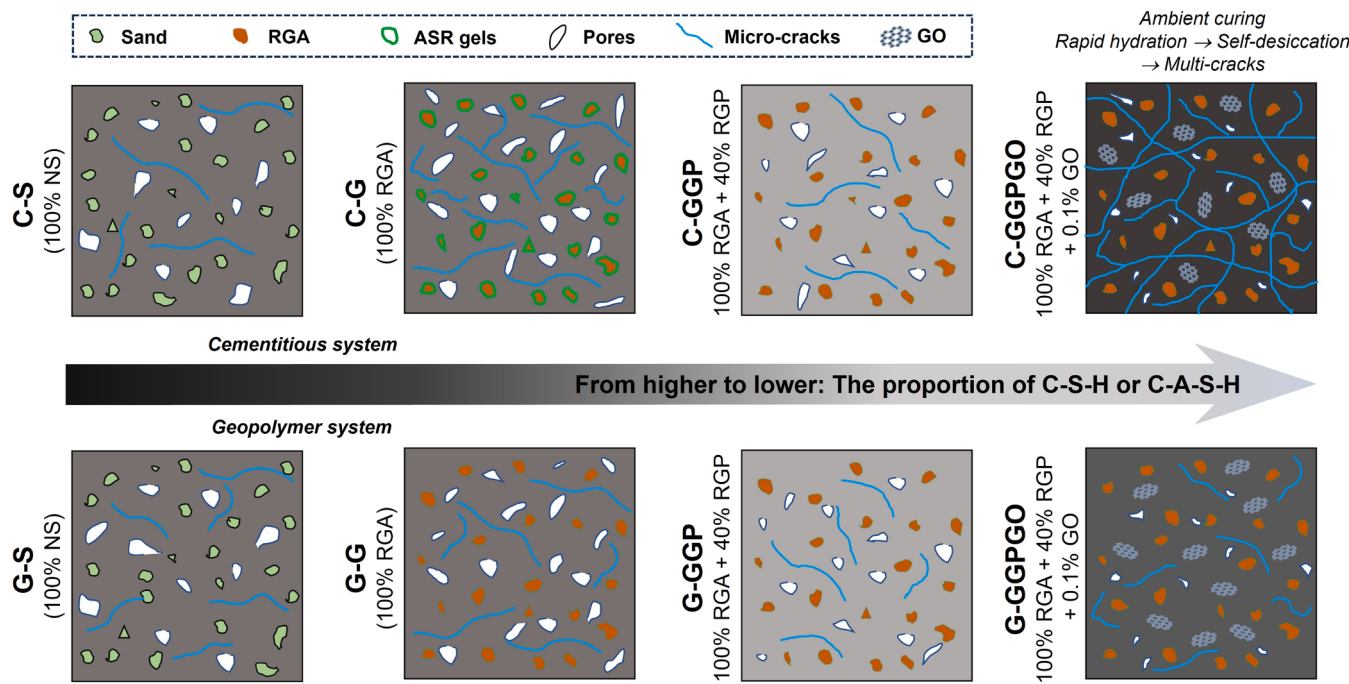


Fig. 14. The combined effects of RGA, RGP and GO on the microstructure of both cementitious and geopolymer matrices under ambient curing condition.

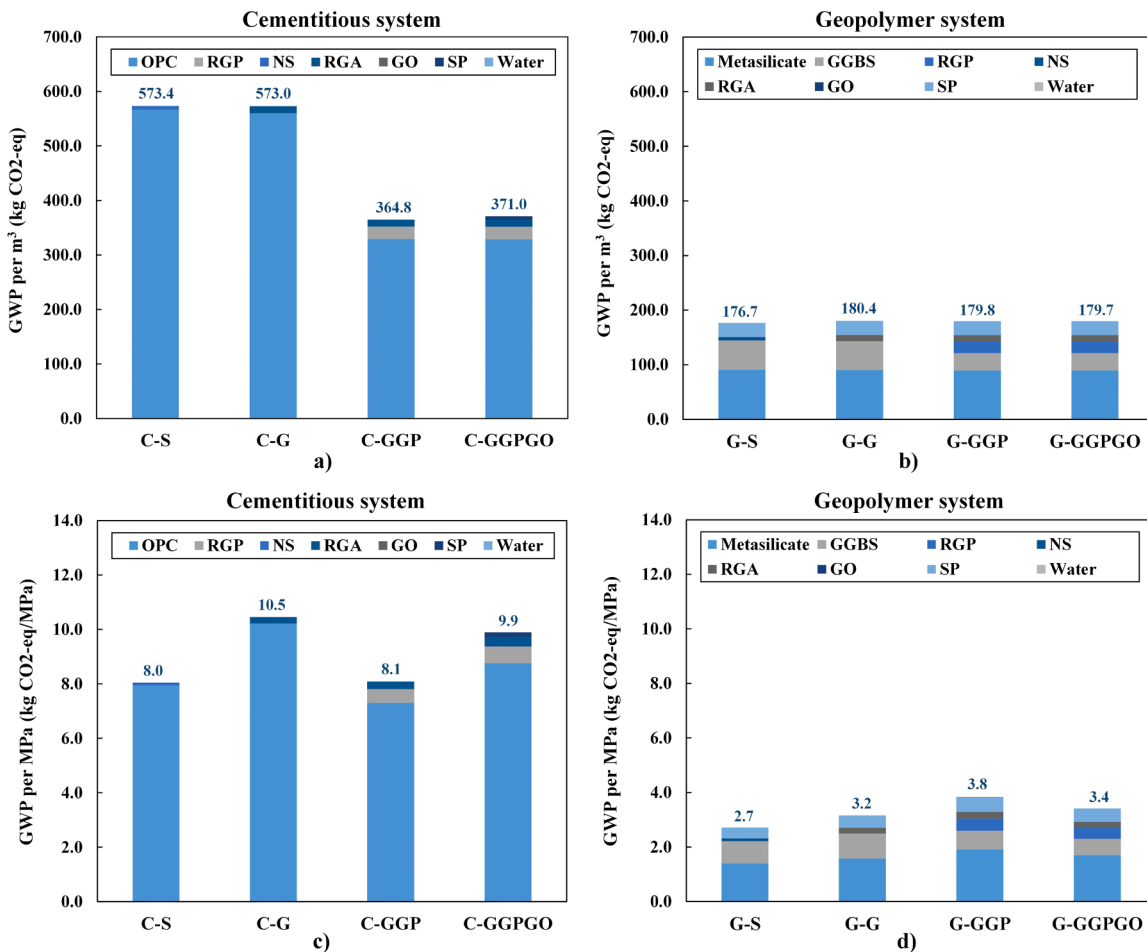


Fig. 15. GWP (kg CO<sub>2</sub>-eq) of cementitious materials (left) and geopolymer materials (right): (a-b) GWP per m<sup>3</sup>, (c-d) GWP per MPa.

growth, thereby refining the pore size, and densifying the microstructure (See Fig. 10). The presence of  $\text{Al}^{3+}$  can reduce the dissolution of amorphous silica in RGP by being incorporated in the silicate network at its surface [125]. As a result, ASR phenomenon in geopolymer system was less pronounced as that in cementitious system.

## 6. Perspectives on sustainability and cost

Fig. 15 presents the breakdown of the carbon footprint of cementitious and geopolymer materials in per  $\text{m}^3$  and per MPa respectively. Generally, cementitious materials exhibit higher embodied carbon (365–573 kg  $\text{CO}_{2\text{-eq}}/\text{m}^3$ ) than the geopolymer ( $\sim 180 \text{ kg CO}_{2\text{-eq}}/\text{m}^3$ ). This is because the majority of the embodied carbon of cementitious system is attributed to OPC, whereas the main contributors to that of geopolymer materials appears to be metasilicate and GGBS. The substitution of sand with RGA fails to mitigate the embodied carbon per  $\text{m}^3$  of mortars, as evidenced in Fig. 15a. Moreover, this substitution engenders an exacerbation of the embodied carbon per MPa of materials (Fig. 15c) due to its adverse impact on compressive strength (see Fig. 4b). However, this approach still has its own merits considering the concurrent issues of waste glass stockpiling and sand shortage. The substitution of 40 wt% of OPC with RGP yields a reduction in embodied carbon by 36 % and 23 % in per  $\text{m}^3$  and per MPa of cementitious mortar respectively, whereas only a slight reduction can be seen in per  $\text{m}^3$  of geopolymer mortar and even 16 % increase per MPa of geopolymer mortar. The introduction of 0.1 wt% GO results in an increased embodied carbon in per MPa of cementitious matrices but a reduction in per MPa of geopolymer mortar due to the opposite effect on their compressive strength. Interestingly,

the total GWP per  $\text{m}^3$  of the geopolymer system remained unchanged despite varying proportions of ingredients in mix designs. Especially, substituting precursors with RGP did not decrease the GWP per  $\text{m}^3$  of the geopolymer mixture.

Fig. 16 presents the breakdown of the cost of cementitious mortars and geopolymer mortars in per  $\text{m}^3$  and per MPa respectively. Comparable cost can be observed between cementitious mortars and of geopolymer mortars, except for the mortars with addition of 0.1 wt% GO. Parallel to the observations on embodied carbon, the replacement of NS with RGA demonstrates an unfavourable impact on cost, simply due to the higher cost of RGA compared to NS on the current market. The incorporation of RGP leads to a cost reduction in per  $\text{m}^3$  of cementitious/geopolymer mortar but an increase in per MPa of cementitious/geopolymer mortar. Similar to the findings in embodied carbon, the introduction of 0.1 wt% GO results in a 34 % cost increase in per MPa of cementitious mortar but a 4 % reduction in that of geopolymer mortar due to the opposite effect on compressive strength.

## 7. Concluding remarks

This study demonstrates the viability of incorporating high-volume recycled glass materials—constituting over 70 wt% of the mixture—into both cementitious and geopolymer systems. Specifically, RGA was used as a complete (100 %) replacement for natural sand, RGP as 40 wt% of the binder in cementitious system and the precursors in geopolymer system, and 0.1 wt% GO was included as a nano-scale reinforcement. The individual and combined effects of these materials were evaluated based on key engineering performance metrics,

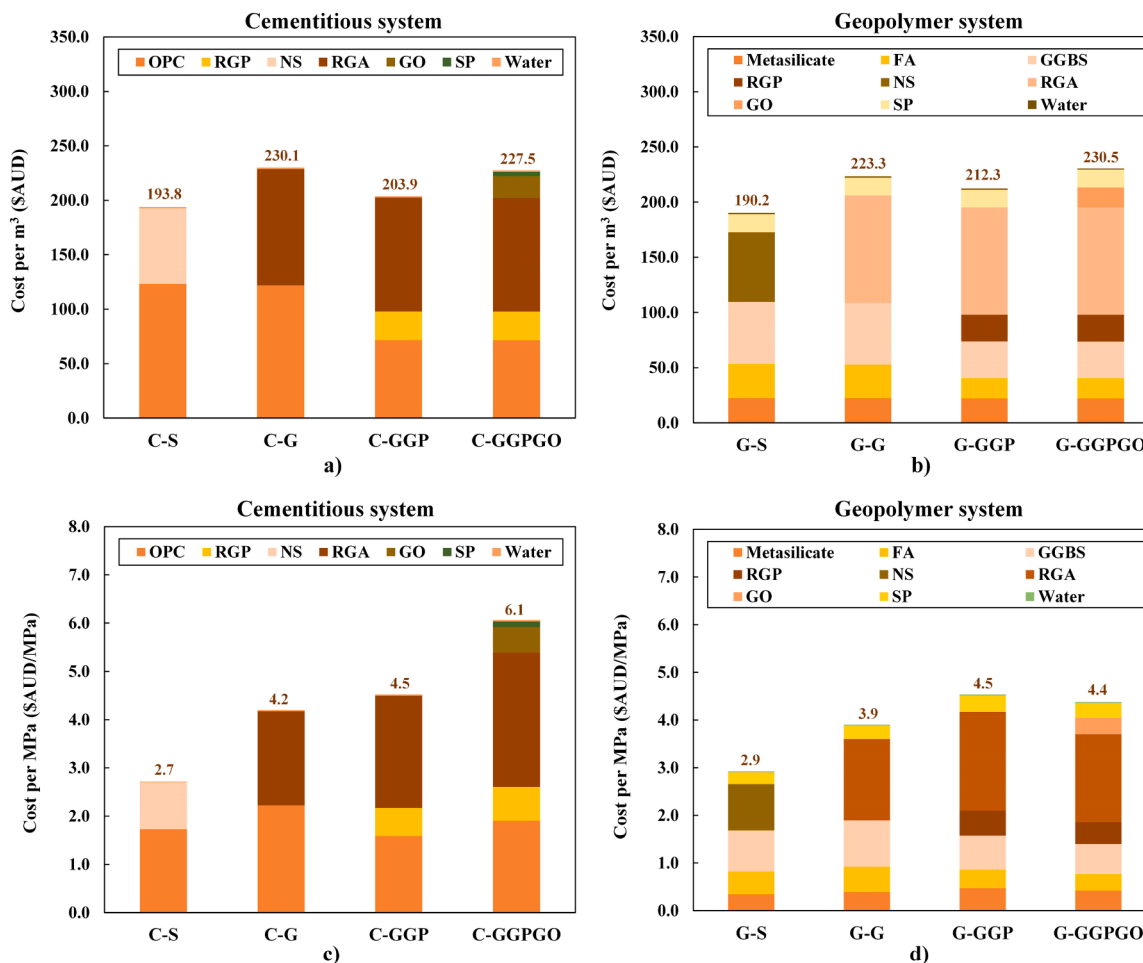


Fig. 16. Cost (\$AUD) of cementitious materials (left) and geopolymer materials (right): (a-b) Cost per  $\text{m}^3$ , (c-d) Cost per MPa.

including workability, compressive strength, and ASR expansion. The study also assessed the reaction kinetics and microstructure of both cementitious and geopolymers systems. In addition, a comparative analysis of the environmental impact and cost was performed for the mortars under investigation. The key research findings are summarized as follows:

#### For cementitious system

- Completely replacing sand with RGA reduces strength by 23 % and exacerbates ASR, leading to expansions five times above the 0.1 % limit.
- Substituting 40 % cement with RGP lowers strength but effectively mitigates ASR, by reducing OH<sup>-</sup> concentration and limiting alkali ingress.
- Although GO accelerates C-S-H gel formation and creates a denser ITZ, it did not improve strength due to self-desiccation and micro-cracking under ambient curing. Therefore, its use is not recommended without guaranteed good curing conditions.
- RGA replacement matches CO<sub>2</sub> emissions but increases costs. Using 40 wt% RGP cuts CO<sub>2</sub> emissions by 36.4 %, while adding GO raises costs without performance gains.

#### For geopolymers system

- The presence of RGP increases Na<sup>+</sup> concentration, enhancing the dissolution of reactive Si and Al species, but limited Al species in RGP restricts C-(A)-S-H gel formation, leading to lower compressive strength. The inclusion of GO enhanced strength by accelerating geopolymersation.
- Geopolymer mortar exhibit extremely lower ASR expansion due to the superb alkali-binding capacity of N-A-S-H/C-A-S-H gels and denser ITZ, reducing the availability of free alkalis for ASR. Both RGP and GO demonstrate beneficial effects on ASR suppression.
- Geopolymer systems exhibit a significantly lower GWP of less than 180 kg CO<sub>2</sub>-eq/m<sup>3</sup> compared to cementitious systems, while maintaining a comparable cost of 190–230 AUD/m<sup>3</sup>.

## 8. Limitation and recommendations

While this research successfully demonstrates the potential of incorporating high volume recycled glass and GO into cementitious and geopolymers composites, one of the key limitations is its reliance on controlled laboratory conditions, which may not fully replicate the complexities of real-world construction environments. This raises questions about the scalability and practical application of these materials in diverse construction scenarios. Moreover, the performance under varying environmental conditions and the long-term durability of these materials also remains uncertain, highlighting the need for further research in these areas.

To address these limitations, future studies should prioritise conducting field trials to evaluate the performance of the high-volume recycled glass composites in real-world conditions. Investigating the long-term durability, with a focus on potential microstructural changes, will be crucial for ensuring their viability over extended periods. Additionally, research should explore the scalability of production methods to ensure that these innovative materials can be produced cost-effectively for large-scale construction projects. A comprehensive life cycle assessment of these composites will further establish their sustainability credentials. Finally, assessing the compatibility of these composites with other construction materials and techniques will enhance their integration into existing practices, paving the way for broader adoption in the construction industry.

## CRediT authorship contribution statement

**Nghia Tran:** Writing – original draft, Validation, Methodology,

Investigation, Formal analysis, Data curation. **Hesong Jin:** Writing – original draft, Visualization, Formal analysis. **Tuan Ngo:** Writing – review & editing, Supervision, Project administration. **Tianchun Wang:** Writing – original draft, Methodology, Investigation, Formal analysis, Data curation, Conceptualization. **Tuan Nguyen:** Writing – review & editing, Validation, Supervision, Resources, Project administration, Methodology, Investigation, Funding acquisition, Formal analysis, Conceptualization.

## Declaration of Competing Interest

The authors declare that they have no known competing financial interests or personal relationships that could have appeared to influence the work reported in this paper.

## Data availability

Data will be made available on request.

## Acknowledgement

The second and third authors (TW and TN) acknowledge the MCF-CRX grant funding from The University of Melbourne that enabled this research. The authors also appreciate Dr. Yulin Patrisia for the technical support in conducting FTIR and TGA. Special thanks to the Materials Characterisation and Fabrication Platform (MCFP) and the Ian Holmes Imaging Centre – Bio21 Institute for providing access to XRD and SEM/EDS.

## References

- [1] M.N.N. Khan, A.K. Saha, P.K. Sarker, Reuse of waste glass as a supplementary binder and aggregate for sustainable cement-based construction materials: a review, *J. Build. Eng.* 28 (2020) 101052.
- [2] P. Guo, et al., New perspectives on recycling waste glass in manufacturing concrete for sustainable civil infrastructure, *Constr. Build. Mater.* 257 (2020) 119579.
- [3] I.B. Topcu, M. Canbaz, Properties of concrete containing waste glass, *Cem. Concr. Res.* 34 (2) (2004) 267–274.
- [4] T. Wang, et al., Sustainable utilisation of low-grade and contaminated waste glass fines as a partial sand replacement in structural concrete, *Case Stud. Constr. Mater.* 16 (2022) e00794.
- [5] Agency, U.S.E.P., Advancing Sustainable Materials Management: 2015 Fact Sheet. 2018: Washington D.C.
- [6] Hong Kong, Monitoring of Solid Waste in Hong Kong: Waste Statistics for 2016. 2017.
- [7] W. Dong, W. Li, Z. Tao, A comprehensive review on performance of cementitious and geopolymers concretes with recycled waste glass as powder, sand or cullet, *Resour. Conserv. Recycl.* 172 (2021) 105664.
- [8] K.I.M. Ibrahim, Recycled waste glass powder as a partial replacement of cement in concrete containing silica fume and fly ash, *Case Stud. Constr. Mater.* 15 (2021).
- [9] N. Tamanna, R. Tuladhar, N. Sivakugan, Performance of recycled waste glass sand as partial replacement of sand in concrete, *Constr. Build. Mater.* 239 (2020) 117804.
- [10] P.J. Monteiro, S.A. Miller, A. Horvath, Towards sustainable concrete, *Nat. Mater.* 16 (7) (2017) 698–699.
- [11] T. Wang, et al., Experimental and numerical study of long-term alkali-silica reaction (ASR) expansion in mortar with recycled glass, *Cem. Concr. Compos.* 139 (2023) 105043.
- [12] T. Wang, et al., Mechanical behaviour of glass-mortar under uniaxial compression loading based on a meso-scale modelling approach, *Constr. Build. Mater.* 359 (2022) 129499.
- [13] Y. Jiang, et al., A critical review of waste glass powder – multiple roles of utilization in cement-based materials and construction products, *J. Environ. Manag.* 242 (2019) 440–449.
- [14] A.M. Rashad, Recycled waste glass as fine aggregate replacement in cementitious materials based on Portland cement, *Constr. Build. Mater.* 72 (2014) 340–357.
- [15] Y. Jiang, et al., A critical review of waste glass powder - multiple roles of utilization in cement-based materials and construction products, *J. Environ. Manag.* 242 (2019) 440–449.
- [16] Q. Li, et al., Performance of waste glass powder as a pozzolanic material in blended cement mortar, *Constr. Build. Mater.* 324 (2022) 126531.
- [17] K. Zheng, Pozzolanic reaction of glass powder and its role in controlling alkali-silica reaction, *Cem. Concr. Compos.* 67 (2016) 30–38.

- [18] K. Afshinnia, P.R. Rangaraju, Influence of fineness of ground recycled glass on mitigation of alkali-silica reaction in mortars, *Constr. Build. Mater.* 81 (2015) 257–267.
- [19] R. Xiao, et al., A state-of-the-art review of crushed urban waste glass used in OPC and AAMs (geopolymer): Progress and challenges, *Clean. Mater.* 4 (2022) 100083.
- [20] S.G. Gok, O. Sengul, Mechanical properties of alkali-activated slag based SIFCON incorporating waste steel fibers and waste glass, *Constr. Build. Mater.* 408 (2023) 133697.
- [21] S.G. Gok, O. Sengul, The use of waste glass as an activator in alkali-activated slag mortars. Proceedings of the Institution of Civil Engineers-Engineering Sustainability, Thomas Telford Ltd, 2020.
- [22] H. Du, K.H. Tan, Concrete with recycled glass as fine aggregates, *Acids Mater.* J. 111 (1) (2014) 47–57.
- [23] W. Jin, C. Meyer, S. Baxter, Glascrete-Concrete with glass aggregate, *Acids Mater.* J. (2000).
- [24] F. Rajabipour, H. Maraghechi, G. Fischer, Investigating the alkali-silica reaction of recycled glass aggregates in concrete materials, *J. Mater. Civ. Eng.* 22 (12) (2010) 1201–1208.
- [25] Z. Xie, W. Xiang, Y. Xi, ASR potentials of glass aggregates in water-glass activated fly ash and portland cement mortars, *J. Mater. Civ. Eng.* 15 (1) (2003) 67–74.
- [26] T. Wang, et al., Experimental and numerical study of long-term alkali-silica reaction (ASR) expansion in mortar with recycled glass, *Cem. Concr. Compos.* 139 (2023) 105043.
- [27] A. Siddika, et al., Waste glass in cement and geopolymer concretes: a review on durability and challenges, *Polymers* 13 (13) (2021) 2071.
- [28] W. Wang, T. Noguchi, Alkali-silica reaction (ASR) in the alkali-activated cement (AAC) system: a state-of-the-art review, *Constr. Build. Mater.* 252 (2020) 119105.
- [29] R. Xiao, et al., Toward waste glass upcycling: preparation and characterization of high-volume waste glass geopolymers composites, *Sustain. Mater. Technol.* 40 (2024) e00890.
- [30] K. Afshinnia, P.R. Rangaraju, Impact of combined use of ground glass powder and crushed glass aggregate on selected properties of Portland cement concrete, *Constr. Build. Mater.* 117 (2016) 263–272.
- [31] S. Liu, et al., Inhibitory effect of waste glass powder on ASR expansion induced by waste glass aggregate, *Materials* 8 (10) (2015) 6849–6862.
- [32] A. Shayan, A. Xu, Performance of glass powder as a pozzolanic material in concrete: a field trial on concrete slabs, *Cem. Concr. Res.* 36 (3) (2006) 457–468.
- [33] J.-X. Lu, et al., Co-utilization of waste glass cullet and glass powder in precast concrete products, *Constr. Build. Mater.* 223 (2019) 210–220.
- [34] N.P. Tran, et al., High-temperature stability of ambient-cured one-part alkali-activated materials incorporating graphene nanoplatelets for thermal energy storage, *Dev. Built Environ.* 18 (2024) 100447.
- [35] L. Zhao, et al., An intensive review on the role of graphene oxide in cement-based materials, *Constr. Build. Mater.* 241 (2020) 117939.
- [36] J. Luo, et al., Using graphene oxide to improve physical property and control ASR expansion of cement mortar, *Constr. Build. Mater.* 307 (2021) 125006.
- [37] C. Liu, et al., Review on the research progress of cement-based and geopolymers materials modified by graphene and graphene oxide, *Nanotechnol. Rev.* 9 (1) (2020) 155–169.
- [38] W.-J. Long, et al., Evaluation of the inhibiting effect of graphene oxide on lead leaching from waste cathode-ray tube glass incorporated in cement mortar, *Cem. Concr. Compos.* 104 (2019) 103337.
- [39] W.-J. Long, et al., Utilization of graphene oxide for improving the environmental compatibility of cement-based materials containing waste cathode-ray tube glass, *J. Clean. Prod.* 192 (2018) 151–158.
- [40] Z.T. Yao, et al., A comprehensive review on the applications of coal fly ash, *Earth-Sci. Rev.* 141 (2015) 105–121.
- [41] T. Hemalatha, A. Ramaswamy, A review on fly ash characteristics—towards promoting high volume utilization in developing sustainable concrete, *J. Clean. Prod.* 147 (2017) 546–559.
- [42] C.-q. Wang, et al., Utilization of fly ash as building material admixture: basic properties and heavy metal leaching, *Case Stud. Constr. Mater.* 17 (2022) e01422.
- [43] I. Kilic, S.G. Gok, A study on investigating the properties of alkali-activated roller compacted concretes, *Adv. Concr. Constr.* 12 (2) (2021) 117–123.
- [44] S.G. Gökk, I. Kilic, Ö. Sengül, Properties of alkali-activated roller compacted concretes produced from waste aggregates. *Cem. -Wapno-Beton= Cem. Lime Concr.* 26 (4) (2022) 352–363.
- [45] J.M. Paris, et al., A review of waste products utilized as supplements to Portland cement in concrete, *J. Clean. Prod.* 121 (2016) 1–18.
- [46] I. Diaz-Loya, et al., Extending supplementary cementitious material resources: reclaimed and remediated fly ash and natural pozzolans, *Cem. Concr. Compos.* 101 (2019) 44–51.
- [47] D.L. Gray, Decrease in fly ash spurring innovation within construction materials industry, *Nat. Gas. Electr.* 35 (6) (2019) 23–29.
- [48] K. Scrivener, et al., Calcined clay limestone cements (LC3), *Cem. Concr. Res.* 114 (2018) 49–56.
- [49] R. Snellings, Assessing, understanding and unlocking supplementary cementitious materials, *RILEM Tech. Lett.* 1 (2016) 50–55.
- [50] M.D. Gavrilletea, Environmental impacts of sand exploitation. Analysis of sand market, *Sustainability* 9 (7) (2017) 1118.
- [51] N. Tran, T. Nguyen, T. Ngo, On The Potential Use of Copper-Modified Geopolymer Incorporating Lead-Smelter Slag for Thermal Energy Storage. SolarPACES Conference Proceedings, TIB Open Publishing, Sydney, Australia, 2024.
- [52] G. Habert, et al., Environmental impacts and decarbonization strategies in the cement and concrete industries, *Nat. Rev. Earth Environ.* 1 (11) (2020) 559–573.
- [53] M. Schneider, et al., Sustainable cement production—present and future, *Cem. Concr. Res.* 41 (7) (2011) 642–650.
- [54] Solutions, M.B. 2024; Available from: <https://master-builders-solutions.com/en-au/products/mastergleniumsky/masterglenium-sky-8379/>.
- [55] ASTM, ASTM C1260-21, Standard Test Method for Potential Alkali Reactivity of Aggregates (Mortar-Bar Method), ASTM International, West Conshohocken, PA, 2021.
- [56] N.P. Tran, et al., Upcycled polypropylene and polytrimethylene terephthalate carpet waste in reinforcing cementitious composites, *Acids Mater.* J. 119 (4) (2022).
- [57] ASTM, ASTM C 1437, Standard Test Method for Flow of Hydraulic Cement Mortar., ASTM International, West Conshohocken, PA, 2013.
- [58] ASTM, ASTM C109/C109M-20 Standard Test Method for Compressive Strength of Hydraulic Cement Mortars (Using 2-in. or [50-mm] Cube Specimens). 2020.
- [59] ASTM, ASTM C1567, Standard Test Method for Determining the Potential Alkali-Silica Reactivity of Combinations of Cementitious Materials and Aggregate (Accelerated Mortar-Bar Method). ., ASTM International, West Conshohocken, PA, 2021.
- [60] N.P. Tran, Performance of Sustainable Fibre Reinforced Cementitious Composite Incorporating Recycled Synthetic Textile Waste, RMIT University, 2021.
- [61] N.P. Tran, et al., Repurposing of blended fabric waste for sustainable cement-based composite: mechanical and microstructural performance, *Constr. Build. Mater.* 362 (2023) 129785.
- [62] N.P. Tran, et al., Utilization of recycled fabric-waste fibers in cementitious composite, *J. Mater. Civ. Eng.* (2022).
- [63] R.K. Pachauri, A. Reisinger, IPCC fourth assessment report, 2007, IPCC, Geneva, 2007 044023.
- [64] T. Grant, H. Rocha, AusLCA (Australian National Life Cycle Inventory) Database\_V1.42, Australian LCA Society (ALCAS), 2023.
- [65] P. Vu Hong Son, et al., Steel slag aggregate low-cement concrete: engineering performance, microstructure and sustainability, *Constr. Build. Mater.* 436 (2024) 136827.
- [66] P. Zandifaez, et al., AI-Assisted optimisation of green concrete mixes incorporating recycled concrete aggregates, *Constr. Build. Mater.* 391 (2023).
- [67] Minerals, V., Environmental Product Declaration (EPD) for thee Ground Glass Pozzolans produced from E-glass at Vitro Minerals' Jackson Plant. 2021.
- [68] E.L. Tucker, et al., Economic and life cycle assessment of recycling municipal glass as a pozzolan in portland cement concrete production, *Resour., Conserv. Recycl.* 129 (2018) 240–247.
- [69] Boral, Bulk Cement and Cementitious Products EPD Environmental Product Declaration Victoria (VIC) region. 2023.
- [70] T.-A. Kua, et al., Environmental and economic viability of Alkali Activated Material (AAM) comprising slag, fly ash and spent coffee ground, *Int. J. Sustain. Eng.* 12 (4) (2018) 223–232.
- [71] Y. Patrisia, et al., Life cycle assessment of alkali-activated concretes under marine exposure in an Australian context, *Environ. Impact Assess. Rev.* 96 (2022).
- [72] Q. Tushar, et al., Application of recycled crushed glass in road pavements and pipeline bedding: an integrated environmental evaluation using LCA, *Sci. Total Environ.* 881 (2023) 163488.
- [73] Jordan. Glass Recycling: How to Make Recycled Glass Sand and Bottles. 2023; Available from: Glass Recycling | How to Make Recycled Glass Sand and Bottles .
- [74] M. Cossutta, J. McKechnie, S.J. Pickering, A comparative LCA of different graphene production routes, *Green. Chem.* 19 (24) (2017) 5874–5884.
- [75] 2023; Available from: <https://www.graphenea.com/collections/graphene-oxide-products/highly-concentrated-graphene-oxide-2-5-wt-concentration?variant=41785441058974>.
- [76] P. He, et al., ASR expansion of alkali-activated cement glass aggregate mortars, *Constr. Build. Mater.* 261 (2020) 119925.
- [77] M.N.N. Khan, A.K. Saha, P.K. Sarker, Evaluation of the ASR of waste glass fine aggregate in alkali activated concrete by concrete prism tests, *Constr. Build. Mater.* 266 (2021) 121121.
- [78] J.W. Bullard, et al., Mechanisms of cement hydration, *Cem. Concr. Res.* 41 (12) (2011) 1208–1223.
- [79] M. Antoni, et al., Cement substitution by a combination of metakaolin and limestone, *Cem. Concr. Res.* 42 (12) (2012) 1579–1589.
- [80] S. Adu-Amankwah, et al., Effect of sulfate additions on hydration and performance of ternary slag-limestone composite cements, *Constr. Build. Mater.* 164 (2018) 451–462.
- [81] G. Liu, M.V.A. Florea, H.J.H. Brouwers, The hydration and microstructure characteristics of cement pastes with high volume organic-contaminated waste glass powder, *Constr. Build. Mater.* 187 (2018) 1177–1189.
- [82] C. Pichler, R. Lackner, Post-peak decelerating reaction of Portland cement: monitoring by heat flow calorimetry, modelling by Elovich-Landsberg model and reaction-order model, *Constr. Build. Mater.* 231 (2020) 117107.
- [83] W.L. Lam, et al., Roles of ultra-fine waste glass powder in early hydration of Portland cement: Hydration kinetics, mechanical performance, and microstructure, *Constr. Build. Mater.* 415 (2024) 135042.
- [84] J.-x Lu, Z.-h Duan, C.S. Poon, Fresh properties of cement pastes or mortars incorporating waste glass powder and cullet, *Constr. Build. Mater.* 131 (2017) 793–799.
- [85] Y. Sui, et al., Experimental investigation for the influence of graphene oxide on properties of the cement-waste concrete powder composite, *Constr. Build. Mater.* 276 (2021) 122229.

- [86] V.F.F. Barbosa, K.J.D. MacKenzie, C. Thaumaturgo, Synthesis and characterisation of materials based on inorganic polymers of alumina and silica: sodium polysialate polymers, *Int. J. Inorg. Mater.* 2 (4) (2000) 309–317.
- [87] P. Chindaprasirt, et al., Comparative study on the characteristics of fly ash and bottom ash geopolymers, *Waste Manag.* 29 (2) (2009) 539–543.
- [88] E. Shamsaei, et al., Graphene-based nanosheets for stronger and more durable concrete: a review, *Constr. Build. Mater.* 183 (2018) 642–660.
- [89] T. Tho-In, et al., Compressive strength and microstructure analysis of geopolymer paste using waste glass powder and fly ash, *J. Clean. Prod.* 172 (2018) 2892–2898.
- [90] A. Bouchikhi, et al., Use of residual waste glass in an alkali-activated binder – Structural characterization, environmental leaching behavior and comparison of reactivity, *J. Build. Eng.* 34 (2021) 101903.
- [91] X. Liu, et al., Effects of graphene oxide on microstructure and mechanical properties of graphene oxide-geopolymer composites, *Constr. Build. Mater.* 247 (2020) 118544.
- [92] Z. Zidi, et al., Effect of nano-ZnO on mechanical and thermal properties of geopolymer, *J. Asian Ceram. Soc.* 8 (1) (2020) 1–9.
- [93] O. Burciaga-Díaz, et al., Effect of waste glass incorporation on the properties of geopolymers formulated with low purity metakaolin, *Cem. Concr. Compos.* 107 (2020) 103492.
- [94] W.K.W. Lee, J.S.J. van Deventer, Use of infrared spectroscopy to study geopolymersization of heterogeneous amorphous aluminosilicates, *Langmuir* 19 (21) (2003) 8726–8734.
- [95] Z. Abdollahnejad, et al., Effects of waste ground glass and lime on the crystallinity and strength of geopolymers, *Mag. Concr. Res.* 71 (23) (2019) 1218–1231.
- [96] M.F. Zawrah, et al., Recycling and utilization assessment of waste fired clay bricks (Grog) with granulated blast-furnace slag for geopolymer production, *Process Saf. Environ. Prot.* 103 (2016) 237–251.
- [97] C. Bai, et al., Waste-to-resource preparation of glass-containing foams from geopolymers, *Ceram. Int.* 45 (6) (2019) 7196–7202.
- [98] J. Yang, et al., A novel supplementary cementitious material based on calcined drill cuttings with waste glass to accelerate cement hydration, *Mater. Chem. Phys.* 301 (2023) 127679.
- [99] H. Zhang, et al., Deterioration of ambient-cured and heat-cured fly ash geopolymer concrete by high temperature exposure and prediction of its residual compressive strength, *Constr. Build. Mater.* 262 (2020) 120924.
- [100] Y. Patrisia, et al., The role of Na<sub>2</sub>O dosage in iron-rich fly ash geopolymer mortar, *Arch. Civ. Mech. Eng.* 22 (4) (2022) 181.
- [101] D. Huang, et al., A review and comparison study on drying shrinkage prediction between alkali-activated fly ash/slag and ordinary Portland cement, *Constr. Build. Mater.* 305 (2021) 124760.
- [102] S.B. Park, B.C. Lee, J.H. Kim, Studies on mechanical properties of concrete containing waste glass aggregate, *Cem. Concr. Res.* 34 (12) (2004) 2181–2189.
- [103] B. Taha, G. Nounou, Properties of concrete contains mixed colour waste recycled glass as sand and cement replacement, *Constr. Build. Mater.* 22 (5) (2008) 713–720.
- [104] C. Shi, Corrosion of glasses and expansion mechanism of concrete containing waste glasses as aggregates, *J. Mater. Civ. Eng.* 21 (10) (2009) 529–534.
- [105] S. Yang, H. Cui, C.S. Poon, Assessment of in-situ alkali-silica reaction (ASR) development of glass aggregate concrete prepared with dry-mix and conventional wet-mix methods by X-ray computed micro-tomography, *Cem. Concr. Compos.* 90 (2018) 266–276.
- [106] H. Maraghechi, et al., Effect of calcium on dissolution and precipitation reactions of amorphous silica at high alkalinity, *Cem. Concr. Res.* 87 (2016) 1–13.
- [107] H. Maraghechi, et al., The role of residual cracks on alkali silica reactivity of recycled glass aggregates, *Cem. Concr. Compos.* 34 (1) (2012) 41–47.
- [108] N.P. Tran, et al., A critical review on drying shrinkage mitigation strategies in cement-based materials, *J. Build. Eng.* 38 (2021) 102210.
- [109] T. Ichikawa, Alkali-silica reaction, pessimum effects and pozzolanic effect, *Cem. Concr. Res.* 39 (8) (2009) 716–726.
- [110] A.K. Saha, et al., The ASR mechanism of reactive aggregates in concrete and its mitigation by fly ash: a critical review, *Constr. Build. Mater.* 171 (2018) 743–758.
- [111] P. Shoaei, et al., Glass powder as a partial precursor in Portland cement and alkali-activated slag mortar: a comprehensive comparative study, *Constr. Build. Mater.* 251 (2020).
- [112] R. Siddique, M.I. Khan, *Supplementary Cementing Materials*, Springer Science & Business Media, 2011.
- [113] M. Kamali, A. Ghahremaninezhad, Effect of glass powders on the mechanical and durability properties of cementitious materials, *Constr. Build. Mater.* 98 (2015) 407–416.
- [114] S.C. Paul, B. Šavija, A.J. Babafemi, A comprehensive review on mechanical and durability properties of cement-based materials containing waste recycled glass, *J. Clean. Prod.* 198 (2018) 891–906.
- [115] X. Jiang, et al., Influence of waste glass powder as a supplementary cementitious material (SCM) on physical and mechanical properties of cement paste under high temperatures, *J. Clean. Prod.* 340 (2022) 130778.
- [116] E. Bernard, Y. Yan, B. Lothenbach, Effective cation exchange capacity of calcium silicate hydrates (C-S-H), *Cem. Concr. Res.* 143 (2021) 106393.
- [117] B.J. Zhan, et al., Multi-scale investigation on mechanical behavior and microstructural alteration of C-S-H in carbonated Alite paste, *Cem. Concr. Res.* 144 (2021) 106448.
- [118] S. Zhang, et al., Waste glass as partial mineral precursor in alkali-activated slag/fly ash system, *Cem. Concr. Res.* 102 (2017) 29–40.
- [119] S. Dadsetan, et al., Evaluation of the tridymite formation as a technique for enhancing geopolymer binders based on glass waste, *J. Clean. Prod.* 278 (2021) 123983.
- [120] A. Gladwin Alex, A. Kadir, T. Gebrehiwet Tewele, Review on effects of graphene oxide on mechanical and microstructure of cement-based materials, *Constr. Build. Mater.* 360 (2022) 129609.
- [121] S. Chuah, et al., Nano reinforced cement and concrete composites and new perspective from graphene oxide, *Constr. Build. Mater.* 73 (2014) 113–124.
- [122] Pan, Z., et al., Graphene oxide reinforced cement and concrete, WO Patent App. 2012, PCT/AU2012/001, 582.
- [123] S. Cheng, et al., Influence of industrial-grade graphene oxide on macro and micro properties of ultra-high performance concrete incorporating recycled fine aggregate, *Constr. Build. Mater.* 417 (2024) 135427.
- [124] J. Duchesne, M. Bérubé, The effectiveness of supplementary cementing materials in suppressing expansion due to ASR: another look at the reaction mechanisms part 2: pore solution chemistry, *Cem. Concr. Res.* 24 (2) (1994) 221–230.
- [125] T. Chappex, K.L. Scrivener, The influence of aluminium on the dissolution of amorphous silica and its relation to alkali silica reaction, *Cem. Concr. Res.* 42 (12) (2012) 1645–1649.